Maternal and zygotic gene regulatory effects of endogenous RNAi pathways

Miguel Vasconcelos Almeida[1], António Miguel de Jesus Domingues[1], René F. Ketting[*]

Biology of Non-coding RNA Group, Institute of Molecular Biology, Ackermannweg 4, 55128 Mainz, Germany

[1]Equal contribution

*Correspondence: r.ketting@imb.de

Abstract

Endogenous small RNAs (sRNAs) and Argonaute proteins are ubiquitous regulators of gene expression in germline and somatic tissues. sRNA-Argonaute complexes are often expressed in gametes and are consequently inherited by the next generation upon fertilization. In *Caenorhabditis elegans*, 26G-RNAs are primary endogenous sRNAs that trigger the expression of downstream secondary sRNAs. Two subpopulations of 26G-RNAs exist, each of which displaying strongly compartmentalized expression: one is expressed in the spermatogenic gonad and associates with the Argonautes ALG-3/4; plus another expressed in oocytes and in embryos, which associates with the Argonaute ERGO-1. The determinants and dynamics of gene silencing elicited by 26G-RNAs are largely unknown. Here, we provide diverse new insights into these endogenous sRNA pathways of *C. elegans*. Using genetics and deep sequencing, we dissect a maternal effect of the ERGO-1 branch sRNA pathway. We find that maternal primary sRNAs can trigger the production of zygotic secondary sRNAs that are able to silence targets, even in the absence of zygotic primary triggers. Thus, the interaction of maternal and zygotic sRNA populations, assures target gene silencing throughout

25 animal development. Furthermore, we find that sRNA abundance, the pattern of origin of sRNA and
26 3' UTR length are predictors of the regulatory outcome by the Argonautes ALG-3/4. Lastly, we
27 discovered that ALG-3- and ALG-4-bound 26G-RNAs are dampening the expression of their own
28 mRNAs, revealing a negative feedback loop. Altogether, we provide several new regulatory insights
29 on the dynamics, target regulation and self-regulation of the endogenous RNAi pathways of *C.*
30 *elegans*.

Author Summary

Small RNAs (sRNAs) and their partner Argonaute proteins regulate the expression of target RNAs. When sperm and egg meet upon fertilization, a diverse set of proteins and RNA, including sRNA-Argonaute complexes, is passed on to the developing progeny. Thus, these two players are important to initiate specific gene expression programs in the next generation. The nematode *Caenorhabditis elegans* expresses several classes of sRNAs. 26G-RNAs are a particular class of sRNAs that are divided into two subpopulations: one expressed in the spermatogenic gonad and another expressed in oocytes and in embryos. In this work, we describe the dynamics whereby oogenic 26G-RNAs setup gene silencing in the next generation. We also show several ways that spermatogenic 26G-RNAs and their partner Argonautes, ALG-3 and ALG-4, use to regulate their targets. Finally, we show that ALG-3 and ALG-4 are fine-tuning their own expression, a rare role of Argonaute proteins. Overall, we provide new insights into how sRNAs and Argonautes are regulating gene expression.

Introduction

A plethora of pathways based on non-coding small RNAs (sRNAs) regulate gene expression in every domain of life. These are collectively known as RNA interference (RNAi) or RNAi-like pathways. In invertebrates, which lack adaptive immune systems and interferon response, RNAi-like pathways fulfill an immune role on the nucleic acid level, by controlling viruses and transposable elements (TEs).

MicroRNA (miRNA), Piwi-interacting RNA (piRNA) and endogenous small interfering RNA (endo-siRNA) pathways are the better described RNAi-like pathways, which differ in their biogenesis and specialized cofactors. MicroRNAs are commonly found in many, if not all, tissues and broadly regulate gene expression throughout development (1). piRNAs are typically, but not exclusively, expressed in the metazoan germline, where they assume a central function in TE control (2–5). Endo-siRNA pathways comprise varied classes of sRNAs expressed in the soma and germline that can, for example, control TEs, protein-coding genes and direct heterochromatin formation (6–8). A key commonality of RNAi-like pathways is the participation of Argonaute proteins. These proteins directly associate with sRNAs and Argonaute-sRNA complexes engage transcripts with sequence complementarity, typically resulting in target silencing. sRNA-directed gene silencing can occur both on the post-transcriptional level, by target RNA cleavage and degradation, and/or on the transcriptional level, via nuclear Argonautes that direct heterochromatin formation at target loci.

sRNAs can be viewed as genome guardians against “foreign” nucleic acids (9). In this light, the germline is an important tissue for sRNA production and function to control the transmission of “non-self” genetic elements to progeny. In multiple animals, Piwi-piRNA complexes have been shown to be maternally deposited into zygotes, where they may initiate TE silencing (10–15). Endo-siRNAs are abundantly expressed in gametes, being often required to successfully complete gametogenesis. These may also be deposited into embryos and have roles in setting up gene expression in the next generation. For example in plants, TE-derived endo-siRNAs are abundant in male and female gametes (16). Moreover, endo-siRNAs are expressed in *Drosophila* ovaries (17) and

in mouse oocytes (18,19) to regulate protein-coding genes and TEs. Overall, gamete expression and maternal inheritance of Argonaute-sRNA complexes seem to be a widespread phenomenon in plants and animals, presumably important to tune gene expression during early development.

RNAi was first identified in the nematode *Caenorhabditis elegans* (20). Ever since, *C. elegans* has continuously been an important and fascinating model for studies on RNAi. *C. elegans* has an unprecedented 27 genomically encoded Argonaute genes, comprising a whole worm-specific clade of the Argonaute protein family (21). Several sRNA species have been identified in worms: miRNAs, 21U-RNAs, 22G- and 26G-RNAs (22,23). 21U-RNAs associate with PRG-1, a Piwi class Argonaute, in the germline and are therefore considered the piRNAs of *C. elegans* (24–26). 26G-RNAs can be considered primary endo-siRNAs, in that they elicit production of the overall more abundant secondary endo-siRNA pool, termed 22G-RNAs (27–29).

26G-RNAs are produced by the RNA-dependent RNA Polymerase (RdRP) RRF-3 (27–31). The ERI complex (ERIC) is an accessory complex that assists RRF-3 in producing 26G-RNAs (32–35). The conserved CHHC zinc finger protein GTSF-1 and the Tudor domain protein ERI-5 form a pre-complex with RRF-3 that is responsible for tethering the RdRP to the ERIC (32,35). Two distinct subpopulations of 26G-RNAs are synthesized in the germline and in embryos. One subpopulation is produced in the spermatogenic gonad in L4 hermaphrodites and in the male gonad, where they associate with the redundantly acting paralog Argonautes ALG-3 and ALG-4 (henceforth referred to as ALG-3/4)(27,30,31,34). These 26G-RNAs trigger the biogenesis of secondary 22G-RNAs that have been shown to either promote gene expression through the Argonaute CSR-1 or to inhibit gene expression through unidentified WAGO proteins (27,36). Hence, the effects of ALG-3/4-dependent sRNAs on their targets is complex: while some targets appear to be silenced, the expression of others seems to be positively affected. The regulatory effects resulting of the combined action of ALG-3/4 and CSR-1 seem to be more physiologically relevant at elevated temperatures (36). The conditions determining regulatory outcome, either silencing or licensing, are still unclear.

In the oogenic hermaphrodite gonad and in embryos another subpopulation of 26G-RNAs is produced. These are 3' 2'-O-methylated by the conserved RNA methyltransferase HENN-1 (37–39) and bind to the Argonaute ERGO-1 (29). ERGO-1 targets pseudogenes, recently duplicated genes and long non-coding RNAs (lncRNAs)(29,32,40). It has recently been shown that these targets generally have a small number of introns that lack optimal splicing signals (41). ERGO-1 may thus serve as a surveillance platform to silence these inefficient transcripts, preventing detrimental accumulation of stalled spliceosomes. Effective silencing of these genes is achieved by secondary 22G-RNAs produced after ERGO-1 target recognition (28,29). In turn, these secondary 22G-RNAs may associate with cytoplasmic Argonautes that mediate post-transcriptional gene silencing (29), or to the Argonaute NRDE-3, which is shuttled into the nucleus and further silences its targets on the transcriptional level (42,43).

Depletion of spermatogenic 26G-RNAs, for example in *rrf-3*, *gtsf-1* and *alg-3/4* mutants, results in a range of sperm-derived fertility defects including complete sterility at higher temperatures (27,30–34). The elimination of oogenic/embryonic 26G-RNAs, for example by impairment of *rrf-3*, *gtsf-1* and *ergo-1*, gives rise to an Enhanced RNAi (Eri) phenotype, characterized by a response to exogenous dsRNA that is stronger than in wild-type (21,32–34). This phenotype is thought to reflect competition for common factors between exogenous and endogenous RNAi pathways (33,44). However, this Eri phenotype lacks characterization on the molecular level. Furthermore, a strong maternal rescue was reported for Eri factors (45), suggesting that maternally deposited Eri factors or their dependent sRNAs have an important role in maintaining gene silencing. The basis for this maternal rescue was not further characterized.

In this work, we address a number of gene regulatory aspects of the 26G-RNA pathways in *C. elegans*. First, we genetically dissect a maternal effect displayed by the ERGO-1 branch of the 26G-RNA pathway. Our findings suggest that both maternal and zygotic sRNAs drive gene silencing throughout embryogenesis and larval development until adulthood. Furthermore, we explore ALG-3/4 target regulation and find that sRNA abundance, origin of the sRNAs and 3' UTR length are

120 predictors of the regulatory outcome. Lastly, we find that the 26G-RNA-binding Argonautes ALG-3
121 and ALG-4 negatively regulate their own expression, which, to our knowledge, represents the first
122 description of such regulatory feedback mechanism amongst *C. elegans* Argonautes.

Results

Maternal and zygotic endogenous small RNAs drive RNAi in the soma

rrf-3 and *gtsf-1* mutants lack the two subpopulations of 26G-RNAs, and display the phenotypes associated with depletion of both subpopulations: the enhanced RNAi (Eri) phenotype, shared with *ergo-1* mutants (21,32–34), and sperm-derived fertility defects, shared with *alg-3/4* double mutants (27,30–34,36). **S1A Fig** offers a simplified scheme of these pathways. For clarity, the two subpopulations of 26G-RNAs and downstream 22G-RNAs, dependent on ERGO-1 or ALG-3/4 will be referred to as ERGO-1 branch sRNAs and ALG-3/4 branch sRNAs, respectively.

We have previously shown that germline-specific GTSF-1 transgenes could rescue the enhanced RNAi (Eri) phenotype of *gtsf-1* mutants (32). This was an intriguing result, since the Eri phenotype arises after targeting somatically expressed genes with RNAi, indicating that germline-expressed GTSF-1 is able to affect RNAi in the soma, possibly through maternal deposition of GTSF-1 or GTSF-1-dependent sRNAs. We reasoned that if maternal GTSF-1 activity can prime gene silencing in embryos then the transmission of the Eri phenotype should show a maternal rescue. To address this experimentally, we linked *gtsf-1(xf43)* to *dpy-4(e1166)*, and crossed the resulting double mutants with wild-type males (**Fig 1A**). We then allowed for two generations of heterozygosity and assayed for RNAi sensitivity in homozygous *gtsf-1* mutant F1 and F2 generations, scoring for larval arrest triggered by *lir-1* RNAi. Indeed, the Eri phenotype showed a strong maternal effect, arising only in the F2 generation of *gtsf-1* mutants (**Fig 1A**). This is consistent with a maternal effect reported for other Eri factors (45). We have previously shown that GTSF-1 is required to silence a GFP transgene reporting on ERGO-1 branch 22G-RNA activity, referred to as 22G sensor (32). Therefore, we also looked at the dynamics of derepression of this transgene upon introduction of *gtsf-1* mutation. We noticed that strong GFP expression appeared only in the second generation of homozygosity of the *gtsf-1* allele (**Fig 1B-C**). An identical maternal effect on the expression status of this transgene is observed after crossing in *rrf-3*, *ergo-1* and other *gtsf-1* mutant alleles (**S1B Fig**). Combined with our previously described rescue of the Eri phenotype using a germline promoter, these results strongly

149 suggest that maternally provided ERGO-1 branch pathway components are sufficient to establish
150 normal RNAi sensitivity in the soma of *C. elegans*.

151 Although the silencing of the 22G sensor used in our experiments is dependent on ERGO-1,
152 ERGO-1 is not the Argonaute protein binding to the effector 22G-RNA (29,39). This has been shown
153 to be driven by the somatically expressed, nuclear Argonaute protein NRDE-3 (40,42), and maybe
154 additional cytoplasmic WAGOs (29)(**S1A Fig**). In absence of ERGO-1 and other 26G-RNA pathway
155 factors, NRDE-3 is no longer nuclear, and in *nrde-3* mutants the 22G sensor is activated, indicating
156 that NRDE-3 requires sRNA input from ERGO-1 branch sRNAs (32,39,40,42). Strikingly, loss of NRDE-3
157 derepressed the 22G sensor transgene in the first homozygous generation (**Fig 1D**), showing that in
158 contrast to 26G-RNAs, the downstream 22G-RNA pathway is not maternally provided. MUT-16 is a
159 factor required for the nucleation of mutator foci and 22G-RNA biogenesis (46). Confirming the
160 requirement for zygotically produced 22G-RNAs, absence of MUT-16 derepresses the 22G sensor in
161 the first homozygous mutant generation (**Fig 1E**). These results suggest a scenario in which 1) NRDE-3
162 is loaded with zygotically produced 22G-RNAs that are primed by maternally provided 26G-RNAs and
163 2) NRDE-3 activity is maintained in somatic tissues until the adult stage, in absence of a zygotic 26G-
164 RNA pathway.

165 The results presented above show that maternal 26G-RNAs are sufficient for 22G sensor
166 silencing. We also tested whether maternal 26G-RNAs are necessary for 22G sensor silencing by
167 crossing *rrf-3* mutant males with *gtsf-1; 22G sensor* hermaphrodites (**Fig 1F**). Both of these strains
168 lack 26G-RNAs and their downstream 22G-RNAs, therefore, their progeny will not receive a maternal
169 and/or paternal complement of these sRNAs. The 22G sensor was silenced in all cross progeny,
170 showing that in the absence of maternal 26G-RNAs, zygotic 26G-RNAs can induce production of
171 silencing-competent 22G-RNAs. Thus, maternal 26G-RNAs appear to be sufficient but not necessary
172 for target silencing.

173

174 **26G-RNA-derived maternal effects are restricted to the ERGO-1 branch**

175 The maternal effects described above for the Eri phenotype and for 22G sensor silencing, are
176 related to the ERGO-1 branch of the pathway. Next, we wanted to determine if the ALG-3/4 branch
177 also displays such a parental effect. To test this, we assessed the influence of maternal GTSF-1
178 activity on the temperature-sensitive sterility phenotype. Using the same setup as we used for the Eri
179 experiment (in **Fig 1A**), we observe that the temperature-sensitive sperm defect of *gtsf-1* mutants
180 was not rescued maternally (**S1C Fig**), indicating that such maternal effects are likely restricted to the
181 ERGO-1 branch.

182

183 **Maternal GTSF-1 supports zygotic ERGO-1 branch 22G-RNA production**

184 The 22G sensor reports on the silencing activity of a single 22G-RNA that maps to the so-
185 called X-cluster, a known set of targets of ERGO-1 (29,39). Therefore, the experiments above using
186 this 22G sensor have a limited resolution and our observations may not reflect the silencing status of
187 most ERGO-1 targets. To characterize this maternal effect in more detail and in a broader set of
188 ERGO-1 targets, we decided to analyze sRNA populations in young adult animals. Concretely, we
189 outcrossed *dpy-4*; *gtsf-1* and sequenced sRNAs from wild-type and two consecutive generations of
190 Dpy young adult animals (**Fig 2A**). First generation *gtsf-1* homozygous mutants will henceforth be
191 addressed as "mutant F1", and second generation *gtsf-1* homozygous mutants as "mutant F2" (**Fig**
192 **2A**). We sequenced young adult animals because they lack embryos, therefore avoiding confounding
193 effects with zygotic sRNAs of the next generation. sRNAs were cloned and sequenced from four
194 biological replicates. The cloning of sRNAs was done either directly (henceforth referred to as
195 untreated samples) or after treatment with the pyrophosphatase RppH (47) before library
196 preparation. The latter enriches for 22G-RNA species that bear a 5' triphosphate group. Sequenced
197 sRNAs were normalized to all mapped reads excluding structural reads (sequencing statistics can be

198 found in the **S1 Table**). In our analysis we strictly looked at 26G- and 22G-RNAs that map in antisense
199 orientation to protein-coding and non-coding genes (see **Methods**).

200 Total 26G-RNA levels are depleted in young adults lacking GTSF-1 (**Fig 2B**). Mutant F1s have
201 significantly less 26G-RNAs than wild-type worms, while mutant F2s have 26G-RNA levels very close
202 to zero (**Fig 2B**). For a finer analysis we looked specifically at 26G-RNAs derived from ERGO-1 and
203 ALG-3/4 targets (as defined in reference 32, see **Methods**). 26G-RNAs mapping to these two sets of
204 targets recapitulate the pattern observed for global 26G-RNAs (**Fig 2C-D**). The difference between
205 the F1 and F2 mutants might reflect a maternal 26G-RNA pool that is still detectable in the young
206 adult F1, but no longer in the F2. However, we point out that amongst the selected F1 Dpy animals,
207 approximately 5.2% will in fact be *gtsf-1* heterozygous, due to meiotic recombination between *gtsf-1*
208 and *dpy-4* (estimated genetic distance between these two genes is 2.6 map units). Hence, another
209 explanation for the mutant F1 pool of 26G-RNAs may be a contamination of the *gtsf-1* homozygous
210 pool with heterozygous animals. The mutant F2 was isolated from genotyped F1 animals, excluding
211 this confounding effect. We conclude that in young adult mutant F1 animals, maternally provided
212 26G-RNAs (or 26G-RNAs produced zygotically by maternal proteins) are no longer detectable at
213 significant levels.

214 Total levels of 22G-RNAs are slightly reduced in mutant F1 and F2 animals (**Fig 2E**). However,
215 total 22G-RNA levels encompass several distinct subpopulations of 22G-RNAs, including those that do
216 not depend on 26G-RNAs. To have a closer look on 22G-RNAs that are dependent on 26G-RNAs, we
217 focused on 22G-RNAs that map to ERGO-1 and ALG-3/4 targets. Strikingly, compared to wild-type,
218 the 22G-RNA population from ERGO-1 targets is moderately higher in mutant F1 animals, and are
219 subsequently depleted in the mutant F2 generation (**Figs 2F and S2A**). These effects are not only
220 clear in overall analysis, but also on a well-established set of ERGO-1 branch targets, such as the X-
221 cluster (**Fig 2G**). Consistent with a role of NRDE-3 downstream of ERGO-1, 22G-RNAs mapping to
222 annotated NRDE-3 targets (43) show the same pattern of depletion as ERGO-1-dependent 22G-RNAs
223 (**S2A Fig**). These results are consistent with the idea that the Eri phenotype and 22G sensor

224 derepression are caused by the absence of NRDE-3-bound, secondary 22G-RNAs downstream of 26G-
225 RNAs.

226 ALG-3/4-dependent downstream 22G-RNAs behave differently in this experiment (**Fig 2H**).
227 Upon disruption of *gtsf-1,* ALG-3/4-dependent 22G-RNAs are only slightly affected in both the
228 mutant F1 and F2 (**Figs 2H and S2A**), despite the fact that their upstream 26G-RNAs are absent. This
229 is illustrated in **S2B Fig** with genome browser tracks of *ssp-16*, a known ALG-3/4 target. We conclude
230 that 26G-RNA-independent mechanisms are in place to drive 22G-RNA production from these genes.

231 Finally, 21U-RNAs and 22G-RNAs mapping to other known RNAi targets are not affected in
232 this inheritance setup, supporting the notion that *gtsf-1* is not affecting these sRNA species (**S2A, C**
233 **Fig**). One exception are the 22G-RNAs from CSR-1 targets, which seem to be slightly depleted in both
234 the mutant F1 and F2 generations (**S2A Fig**). It is not possible to dissect whether this is a direct effect
235 or not, but we note that mRNA levels of CSR-1 targets are slightly downregulated in the analyzed
236 mutants (**S2D Fig**). Given that CSR-1 22G-RNAs tend to correlate positively with gene expression (48),
237 it is conceivable that the reduction of CSR-1 target 22G-RNAs is the result of decreased target gene
238 expression.

239

240 **ERGO-1 pathway mRNA targets show stronger upregulation in the second *gtsf-1* homozygous**
241 **mutant generation**

242 The very same samples used for generating sRNA sequencing data were also used for mRNA
243 sequencing (**Fig 2A**). First, we checked *gtsf-1* expression. As expected, *gtsf-1* is strongly depleted in
244 the mutant samples (**S3A Fig**). In the mutant F1 we still observe a low level of *gtsf-1* derived
245 transcripts (about 9.5% of wild-type) that is absent from the mutant F2. These transcripts cover the
246 region deleted in the *gtsf-1(xf43)* mutant allele, indicating they cannot represent zygotically
247 transcribed *gtsf-1* mutant mRNA. Rather, they likely come from the above described contamination
248 of the homozygous F1 population with heterozygous animals.

We hypothesized that ERGO-1 branch 22G-RNAs observed in the mutant F1 generation might be competent to maintain target silencing. If this is true, we should observe strong upregulation of ERGO-1 target mRNAs only the mutant F2 generation. Indeed, the X-cluster is upregulated only in the second mutant generation (**Fig 3A**). When ERGO-1 targets are analyzed in bulk, we observe the same trend, with stronger upregulation only in the mutant F2, consistent with the maternal effect (**Fig 3B**). ALG-3/4 targets, as for instance *ssp-16*, were found to be upregulated already in the F1 generation (**Figs 3B** and **S3B**), supporting the notion that the maternal rescue of the 26G-RNA pathways is restricted to the ERGO-1 branch.

Eri targets show stronger expression in embryos

ERGO-1 targets comprise a very diverse set of targets consisting of pseudogenes, fast evolving small genes, paralog genes and lncRNAs (29,40,41). Considering the maternal effect described above for ERGO-1-dependent sRNA and correspondent target, we postulated that this maternal effect may exist to counteract embryonic expression of ERGO-1 targets. To address this we sequenced mRNA of synchronized populations of all developmental stages (L1, L2, L3, L4, young adult and embryos) of both wild-type (N2) and *rrf-3(pk1426)* mutants. Global gene expression in *rrf-3* mutants is significantly different only in embryos (**Fig 3C**, upper panel). These changes may be explained by higher expression of ERGO-1 targets during embryogenesis. Indeed, in wild-type worms, ERGO-1 targets are most abundant in embryos (**Fig 3C**, lower panel, in blue). Moreover, the effect of *rrf-3* mutation on ERGO-1 target expression is stronger in embryos (**Fig 3C**, lower panel). These results indicate that the maternal effect reported above can reflect deposition of factors which are required to initiate silencing of targets early in development.

GTSF-1 is required for sRNA biogenesis and target silencing in the male germline

The young adult sequencing datasets we obtained in this study (**Fig 2A**), as well as previous datasets of gravid adults (32), are not well suited to address ALG-3/4 biology, considering that in these developmental stages ALG-3/4 are not expressed, at least not abundantly. Therefore, in order to further our understanding of the dependency of ALG-3/4 branch sRNAs on GTSF-1, we generated additional sRNA and mRNA datasets from wild-type and *gtsf-1* male animals grown at 20°C.

As expected, global 26G-RNA levels are severely affected in *gtsf-1* mutant males, reflecting downregulation of 26G-RNAs from both branches of the pathway (**Fig 4A-C**). Consistent with the absence of ERGO-1 in adult males, ERGO-1 branch 26G-RNAs are detected in extremely low numbers in wild-type animals (**Fig 4B**). Global levels of 21U-RNAs seem to be moderately augmented (**Fig 4D**), possibly resulting from the lack of 26G-RNAs in the libraries. Global levels of 22G-RNAs are not affected (**Fig 4E**), but consistent with a global depletion of 26G-RNAs, 22G-RNAs specifically mapping to ALG-3/4 and ERGO-1 targets are reduced in *gtsf-1* mutant males (**Fig 4F**). Next, we probed the effects of *gtsf-1* mutation on male gene expression using mRNA sequencing. ALG-3/4 and ERGO-1 targets are both upregulated *gtsf-1* mutant males (**Fig 4G**). These changes are illustrated for the X-cluster and *ssp-16* in the genome browser tracks of **S4 Fig**.

As a final note on the developmental aspects of ALG-3/4 branch, consistent with enrichment in the spermatogenic gonad (27,30–32,34,36), ALG-3/4 targets are more highly expressed and more responsive to *rrf-3* mutation in the L4 and young adult stages of hermaphrodite animals (**Fig 3C**, middle panel). Given that the overall ALG-3/4 target mRNA levels go up upon depletion of *gtsf-1* or *rrf-3* (**Figs 3C** and **4G**), bulk 26G-RNA activity during spermatogenesis seems to be repressive at 20°C.

We conclude that the activity of GTSF-1 is required in the male germline for silencing of 26G-RNA targets by participating in 26G- and 22G-RNA biogenesis.

22G-RNA abundance is a predictor of the regulatory outcome of ALG-3/4 targets

297 ALG-3/4 were shown to have distinct effects on gene expression, either silencing or licensing
298 (27,36). However, how these different effects arise is currently unknown. Even though our analysis in
299 males did not reveal a licensing effect of 26G RNAs, the bulk analysis of targets in **Figs 3B** and **4G** may
300 occlude the behavior of distinct target subpopulations. Of note, our sequencing datasets were
301 obtained from animals grown at 20°C and are therefore blind to the strong positive regulatory effect
302 of ALG-3/4 in gene expression at higher temperatures (36).

303 We reasoned that sRNA abundance may be correlated with different regulatory outcomes.
304 Therefore, we defined ALG-3/4 targets that are upregulated, downregulated and unaltered upon
305 *gtsf-1* mutation and plotted their 26G-RNA abundance. This reveals a tendency for genes that are
306 upregulated upon loss of GTSF-1 to be more heavily targeted by 26G-RNAs in the adult male germline
307 (**Fig 5A**, left panel). The same trend is observed for 22G-RNAs: upregulated genes are more heavily
308 covered by 22G-RNAs (**Fig 5A**, right panel, and **5B**). In contrast, ALG-3/4 targets that are
309 downregulated in *gtsf-1* mutant males display a relatively low-level targeting by 22G-RNAs (**Fig 5A-B**).

310 We conclude that stronger 26G-RNA targeting promotes stronger 22G-RNA biogenesis and
311 repression of targets, whereas low-level targeting by 26G- and 22G-RNAs does not. Transcripts that
312 are downregulated in absence of GTSF-1 might be licensed for gene expression, but may also
313 respond in a secondary manner to a disturbed 26G-RNA pathway.

314

315 **ALG-3/4- and ERGO-1-branch 26G-RNA subpopulations display different patterns of origin that**
316 **influence target expression**

317 It was previously noticed that ALG-3/4-dependent 26G-RNAs mostly map to both the 5' and
318 3' ends of their targets, and that this may correlate with gene expression changes (27). We followed
319 up on this observation by performing metagene analysis of 26G-RNA binding using our broader set of
320 targets. Indeed, ALG-3/4 branch 26G-RNAs display a distinctive pattern with two sharp peaks near
321 the transcription start site (TSS) and transcription end site (TES) (**Figs 6A** and **S5A**, left panels). In

contrast, ERGO-1 branch 26G-RNAs map throughout the transcript, with a slight enrichment in the 3' half (**Figs 6B**, left panel). Contrary to 26G-RNAs, 22G-RNAs from both branches map throughout the transcript (**Figs 6A-B** and **S5A**, right panels). These patterns are consistent with recruitment of RdRPs and production of antisense sRNAs along the full length of the transcript. These findings suggest substantially different regulation modes by ERGO-1- and ALG-3/4-branch 26G-RNAs.

Conine and colleagues reported a correlation between 26G-RNA 5'targeting and negative regulation (27). We wanted to address whether our datasets show concrete correlations between the patterns of origin of ALG-3/4-dependent 26G-RNAs and distinct regulatory outcomes. To address this, we ranked genes by 5' and 3' abundance of 26G-RNAs, selected genes predominantly targeted at the 5' or on the 3' ends and plotted their fold change upon *gtsf-1* mutation. Dominant 5' targeting by 26G-RNAs seems to be correlated with gene silencing (fold change >0 in the mutant, **Fig 6C**), whereas dominant 3' targeting is accompanied with only weak upregulation in *gtsf-1* mutant males (**Fig 6C**). In further support for a non-gene silencing, and potentially licensing role for ALG-3/4 targeting the 3' end, genes with predominant 3' 26G-RNAs display an overall higher expression that genes predominantly targeted on the 5' region (**Fig 6D**). The same signatures are found in young adults, with an even stronger signature of the 3' in promoting gene expression (**S5B-C Fig**).

Finally, we interrogated if the length of 5' and 3' UTRs may be a predictor of regulatory outcome by ALG-3/4. 5' UTR length was not significantly different between unchanged, downregulated and upregulated genes (unpublished observations). In contrast, 3' UTR length is significantly smaller in targets that respond to loss of GTSF-1 in males (**Fig 6E**). Interestingly, we find the same and possibly even stronger relation between 3'UTR length and responsiveness to GTSF-1 status in young adult animals (**S5D Fig**).

Altogether, our results suggest that in males, 3' vs 5' targeting and 3' UTR length are predictors of whether ALG-3/4 targets are silenced or not.

347 **ALG-3 and ALG-4 act in a negative feedback loop**

348 While navigating the lists of GTSF-1 targets defined by differential gene expression analysis,
349 we noticed that *alg-3* and *alg-4* are targets of 26G-RNAs (this study and in reference 32). These 26G-
350 RNAs are sensitive to oxidation (not enriched in oxidized libraries, see reference 32) and map
351 predominantly to the extremities of the transcript (**Figs 7**, upper panels), indicating that these 26G-
352 RNAs share features with ALG-3/4 branch 26G-RNAs. In addition to these 26G-RNAs, significant
353 amounts of 22G-RNAs are found on *alg-3/4* (**Fig 7**, middle panels). These sRNAs seem to silence gene
354 expression, since mRNA-seq shows that *alg-3* and *alg-4* transcripts are 2-3 fold upregulated in *gtsf-1*
355 mutants (**Fig 7**, lower panels).

356 These results strongly suggest that *alg-3/4* are regulating their own expression in a negative
357 feedback loop. Of note, the upregulation of *alg-3* and *alg-4* is in agreement with the results
358 presented above, because these genes are more heavily targeted by 26G-RNAs on their 5' (although
359 *alg-4* also has a sharp 3' 26G-RNA peak, upper panels). Furthermore, these same signatures of
360 negative feedback loop are observed in young adults (**S6 Fig**).

361

362

Discussion

Genetic dissection of a maternal rescue

Animal male and female gametes are rich in RNA. Upon fertilization, several RNA species are thus provided to the zygote. Multiple lines of evidence from several distinct organisms indicate that sRNAs are included in the parental repertoire of inherited RNA. For example, piRNAs have been reported to be maternally deposited in embryos in *D. melanogaster* and *C. elegans* (10,12,13,15,49). In *C. elegans* other endogenous sRNA populations have also been shown to be contributed by the gametes: 1) 26G-RNAs have been shown to be weakly provided by the male, while 22G-RNAs are more abundantly provided (50); 2) 26G-RNAs and the Argonaute ERGO-1 are co-expressed during oogenesis and in embryos (29,31,51); and 3) 22G-RNAs are deposited in embryos via the mother and participate in transgenerational gene silencing (49,52–56).

We describe a maternal effect in the transmission of the Eri phenotype and 22G sensor derepression and characterize the subjacent dynamics of sRNAs and mRNA targets (**Figs 1-3** and **S1-S3**). We show that both maternal and zygotic 26G-RNAs are sufficient for silencing. Absence of either the maternal or the zygotic pools can thus be compensated, enhancing the robustness of this system. We note, however, that sufficiency has only been tested with the described 22G sensor. It may be that the silencing of other targets has differential dependencies on maternal and zygotic 26G-RNA populations. The maternal effect rescue was observed for a variety of Eri genes, including *gtsf-1*, *rrf-3* and *ergo-1*, but not *alg-3/4*. Thus, these defects are related to impairment of sRNA populations directly associated with and downstream of ERGO-1. These results do not exclude a parental effect for ALG-3/4. In fact, a paternal effect on embryogenesis has been described for *rrf-3* mutants (30). Such phenotype most likely arises due to ALG-3/4 branch sRNAs.

Maternal rescue of Eri genes was previously reported (45), although the genetic basis for this phenomenon was not characterized further. We demonstrate that in the first Eri mutant generation, primary 26G-RNAs are downregulated, while their downstream 22G-RNAs are still present (**Fig 2**).

These ERGO-1-dependent 22G-RNAs, maintained in the absence of their primary triggers, seem to be competent to sustain silencing of ERGO-1 targets throughout life of the animal (**Fig 3**). Given that 1) ERGO-1 targets display higher expression during embryogenesis; and 2) upon disruption of endogenous RNAi by *rrf-3* mutation, targets become upregulated in all developmental stages (**Fig 3C**); maternally deposited ERGO-1-dependent factors may be especially required to initiate target silencing during embryogenesis and to prevent spurious expression throughout development. The ERGO-1-independent maintenance of this silencing response may be mechanistically similar to RNA-induced epigenetic silencing (RNAe), involving a self-perpetuating population of 22G-RNAs (49,57,58). Indeed, both processes depend on a nuclear Argonaute protein: HRDE-1 in RNAe (49,57,58) and NRDE-3 for ERGO-1-driven silencing (39,42,43). Self-perpetuating 22G-RNA signals may be also in place in the male germline (see below).

Our genetic experiments and sequencing data are fully consistent with maternal inheritance of 26G-RNAs. However, these may not be the only inherited agent. A non-mutually exclusive idea is that GTSF-1, as well as other ERIC proteins may be deposited in embryos to initiate production of zygotic sRNAs. In accordance with the latter, we have previously demonstrated that formation of the 26G-RNA generating ERIC is developmentally regulated (32). While in young adults there is a comparable amount of pre- and mature ERIC, in embryos there is proportionally more mature ERIC. These observations suggest that pre-ERIC might be deposited in the embryo to swiftly jumpstart zygotic 26G-RNA expression after fertilization.

26G-RNAs act as triggers to induce a self-sustained 22G-RNA-driven silencing in the male germline

We show that GTSF-1 is required in adult males to produce 26G- and downstream 22G-RNAs (**Fig 4**) analogous to its role in the hermaphrodite germline and in embryos (32). In addition, the bulk of targets from both 26G-RNA pathway branches seem to be deregulated. Interestingly, we note that although ERGO-1 and its cognate 26G-RNAs are not abundantly expressed in spermatogenic tissues

413 (**Fig 4B**), *gtsf-1*-dependent, secondary 22G-RNAs mapping to these genes maintain gene silencing in
414 the male germline (**Fig 4F-G**). In an analogous manner, we find that ALG-3/4 targets maintain 22G-
415 RNAs in gravid adults (32), even though ALG-3/4 is not expressed at that stage. Mechanistically this
416 may be closely related to how maternal 26G-RNAs can trigger 22G-RNA-driven silencing (see above).
417 NRDE-3 is downstream of ERGO-1, likely silencing ERGO-1 targets throughout development.
418 However, the Argonautes associated with 22G-RNAs mapping to 1) ERGO-1 targets in the male, and
419 2) to ALG-3/4 targets in gravid adults have not yet been identified.

420

421 **Two distinct ALG-3/4 regulatory mechanisms?**

422 ALG-3/4-branch 26G-RNAs map very sharply to the 5' and 3' extremities of the targets, very
423 close to the transcription start and end sites. We find that stronger targeting on the 3' end does not
424 drive robust gene silencing, and may even license expression, while targeting on the 5' end is
425 associated with stronger gene silencing. Targeting on the 3' is consistent with RdRP recruitment to
426 synthesize antisense secondary 22G-RNAs throughout the transcript. These may associate with CSR-1
427 and could have a positive effect on gene expression. The sharp 5' peak in the metagene analysis
428 could hint at additional regulatory modes, other than 22G-RNA targeting. 5'-end-bound ALG-3/4
429 could recruit other effector factors which promote RNA decay or translation inhibition, e.g. by
430 inhibiting the assembly of ribosomes. Of note, when single targets are considered individually, 26G-
431 RNA peaks at 5' and 3' can be simultaneously detected (**Figs 7**, **S2B** and **S5A**, left panels and **S6**).
432 Hence, the resolution of a balance between Argonaute-sRNA complexes binding at 5' and 3' could
433 determine regulatory outcome. Notably, we find shorter 3' UTRs to be correlated with gene silencing
434 (**Fig 6E**). In a model where predominant 3' UTR targeting by Argonaute-sRNA complexes promotes
435 gene expression, shorter 3' UTRs and therefore less chance of sRNA binding may shift the balance
436 towards gene silencing. Another possibility may be that longer 3' UTRs contain binding sites for
437 additional RNA binding proteins that may help to restrict RdRP activity on the transcript in question.
438 Further work will be needed to test such ideas.

439

440 **An Argonaute negative feedback loop**

441 In *C. elegans*, primary sRNAs trigger the production of secondary sRNAs in a feedforward
442 loop. If left uncontrolled, such feedforward mechanisms can be detrimental to biological systems.
443 Endogenous and exogenous RNAi pathways in *C. elegans* compete for limiting shared factors and the
444 Eri phenotype is a result of such competition (33,44). Competition for shared factors is in itself a
445 mechanism to limit accumulation of sRNAs. In support of this, exogenous RNAi was shown to affect
446 endogenous sRNA populations, thus restricting the generations over which RNAi effects can be
447 inherited (59).

448 We find that 26G-RNAs, likely ALG-3/4-bound, as well as 22G-RNAs map to *alg-3* and *alg-4*
449 mRNAs (**Figs 7** and **S6**). In the absence of GTSF-1, a loss of these sRNAs is accompanied by a 2-3 fold
450 upregulation of *alg-3* and *alg-4* on the mRNA level. This means that ALG-3 and ALG-4 may regulate
451 their own expression. To the best of our knowledge, this is the first observation in *C. elegans* of
452 Argonaute proteins regulating the expression of their own mRNA, and represents a very interesting
453 case of a break on the positive feedback of the 26G-RNA pathway. Such regulation is not
454 unprecedented. Complementary endo-siRNAs to *ago2* have been described in *Drosophila* S2 cells
455 (60). Since AGO2 is required for the biogenesis and silencing function of endo-siRNAs, it is likely that
456 Ago2 regulates itself in S2 cells.

457 Such direct self-regulation of Argonaute genes may constitute an important mechanism to
458 limit RNAi-related responses, but the biological relevance of this regulation will need to be addressed
459 experimentally. These observations do suggest that the Eri phenotype is but one manifestation of
460 intricate cross-regulation governing the RNAi pathways of *C. elegans*.

461

462

463

464

Materials and Methods

C. elegans genetics and culture

C. elegans was cultured on OP50 bacteria according to standard laboratory conditions (61). Unless otherwise noted, worms were grown at 20°C. The Bristol strain N2 was used as the standard wild-type strain. All strains used and created in this study are listed in **S2 Table**.

Microscopy

Wide-field photomicrographs were acquired using a Leica M165FC microscope with a Leica DFC450 C camera, and were processed using Leica LAS software and ImageJ.

Genetic crosses using *dpy-4;gtsf-1* worms

Cross outline. We first linked *gtsf-1(xf43)* and *dpy-4(e1166)*. These genes are 2.62 cM apart, which does not comprise extremely tight linkage. Therefore, throughout the outcrossing scheme, worms were consistently genotyped for *gtsf-1* and phenotyped for *dpy-4*. We started by outcrossing *dpy-4;gtsf-1* hermaphrodites with N2 males (in a 1:2 ratio). *dpy-4(e1166)* is reported as being weakly semi-dominant (https://cgc.umn.edu/strain/CB1166). Indeed, heterozygote worms look only very slightly Dpy, therefore for simplicity, we refer to the heterozygote phenotype as "wild-type" throughout this work. Wild-type looking worms were selected in the F1 and F2 generations. The F2s were allowed to lay embryos for 1-2 days and then were genotyped for *gtsf-1(xf43)* using PCR. Progenies of non-recombined *gtsf-1* heterozygote worms were kept for follow up. F3 progenies that did not segregate *dpy* worms were discarded. F3 *dpys* were isolated, allowed to lay embryos, and genotyped for *gtsf-1(xf43)*. Progenies of non-homozygote mutant *gtsf-1(xf43)* worms were discarded.

RNAi. dsRNA against *lir-1* was supplemented to worms by feeding as described (62). L1 worms were transferred to RNAi plates and larval arrest was scored 2-3 days later. L1 F3 and F4 worms were transferred to RNAi plates blinded to genotype/phenotype (the *dpy* phenotype only shows clearly from L3 onwards).

Temperature-sensitive sterility assay. Single L1 F3 and F4 worms were transferred to OP50 plates, blinded to genotype/phenotype and grown at 25^{o}C (the *dpy* phenotype only shows clearly from L3 onwards). Temperature sensitive-sterility was scored on the second day of adulthood and worms with unexpected genotype-phenotype were genotyped for *gtsf-1*.

RNA isolation. Approximately 550 hand-picked wild-type, Dpy F3 (referred in the text as mutant F1) and Dpy F4 (referred in the text as mutant F2) animals were used to isolate RNA (see cross description above, schematics in **Fig 2A**, and see below for RNA isolation protocol). Four independent outcrosses were performed and independent biological replicates (of wild-type, mutant F1 and mutant F2) were collected from each. Each sample was used to prepare small RNA and mRNA libraries (see below for details on library preparation).

Growth and RNA isolation of adult males

him-5(e1467) and *him-5(e1467); gtsf-1(xf43)* worm populations were synchronized by bleaching, overnight hatching in M9 and plated on OP50 plates the next day. Worms were grown until adulthood for approximately 73 hours and 400-500 male animals were hand-picked for each sample, in biological triplicates, and used to isolate RNA (see below for RNA isolation protocol). Each sample was used to prepare small RNA and mRNA libraries (see below details on library preparation).

Growth and RNA isolation of N2 and *rrf-3* worms

N2 and *rrf-3(pk1426)* animal populations were synchronized by bleaching, overnight hatching in M9 and plated on OP50 plates the next day. L1 animals were allowed to recover from starvation

for 5 hours, and then were collected. L2 worms were collected 11 hours after plating. L3 animals were collected 28 hours after plating. L4 animals were collected 50 hours after plating, and young adults were collected 56 hours after plating. Embryo samples were collected from bleached gravid adult animals, followed by thorough washes with M9. Samples were collected in triplicate and RNA isolation proceeded as described below.

RNA isolation

Worms were rinsed off plates and washed 4-6 times with M9 supplemented with 0.01% Tween. 50 µL of M9 plus worms were subsequently frozen in dry ice. For RNA isolation worm aliquots were thawed and 500 µL of Trizol LS (Life Technologies, 10296-028) was added and mixed vigorously. Next, we employed six freeze-thaw cycles to dissolve the worms: tubes were frozen in liquid nitrogen for 30 seconds, thawed in a 37^{o}C water bath for 2 minutes, and mixed vigorously. Following the sixth freeze-thaw cycle, 1 volume of 100% ethanol was added to the samples and mixed vigorously. Then, we added these mixtures onto Direct-zol columns (Zymo Research, R2070) and manufacturer's instructions were followed (in-column DNase I treatment was included).

Library preparation for mRNA sequencing

NGS library prep was performed with Illumina's TruSeq stranded mRNA LT Sample Prep Kit following Illumina's standard protocol (Part # 15031047 Rev. E). Starting amounts of RNA used for library preparation, as well as the number of PCR cycles used in amplification, are indicated in **S3 Table**. Libraries were profiled in a High Sensitivity DNA on a 2100 Bioanalyzer (Agilent technologies) and quantified using the Qubit dsDNA HS Assay Kit, in a Qubit 2.0 Fluorometer (Life technologies). Number of pooled samples, Flowcell, type of run and number of cycles used in the different experiments are all indicated in **S3 Table**.

538 **RppH treatment and library preparation for small RNA sequencing**

539 For maternal effect sequencing, RNA was directly used for library preparation, or treated
540 with RppH prior to library preparation. RppH treatment was performed as described in reference 47
541 with slight modifications. In short, 500 ng of RNA were incubated with 5 units of RppH and 10x NEB
542 Buffer 2 for 1 hour at 37°C. Reaction was stopped by incubating the samples with 500 mM EDTA for 5
543 minutes at 65°C. RNA was reprecipitated in 100% Isopropanol and ressuspended in nuclease-free
544 water. NGS library prep was performed with NEXTflex Small RNA-Seq Kit V3 following Step A to Step
545 G of Bioo Scientific`s standard protocol (V16.06). Both directly cloned and RppH-treated libraries
546 were prepared with a starting amount of 200ng and amplified in 16 PCR cycles. Amplified libraries
547 were purified by running an 8% TBE gel and size-selected for 18 – 40 nts. Libraries were profiled in a
548 High Sensitivity DNA on a 2100 Bioanalyzer (Agilent technologies) and quantified using the Qubit
549 dsDNA HS Assay Kit, in a Qubit 2.0 Fluorometer (Life technologies). All 24 samples were pooled in
550 equimolar ratio and sequenced on 1 NextSeq 500/550 High-Output Flowcell, SR for 1x 75 cycles plus
551 6 cycles for the index read.

552 RNA from adult males was RppH-treated as described above with the difference that 800 ng
553 of RNA were used for RppH treatment. Library preparation of these samples was performed exactly
554 as described above with the following modifications: starting amount of 460 ng; and amplification in
555 15 PCR cycles.

556

557 **Bioinformatic analysis**

558 Sequencing statistics can be found in **S1 Table**.

559 *Small RNA read processing and mapping.* Illumina adapters were removed with cutadapt v1.9
560 (63) (-a TGGAATTCTCGGGTGCCAAGG -O 5 -m 26 -M 38) and reads with low-quality calls were filtered
561 out with fastq_quality_filter (-q 20 -p 100 -Q 33) from the FASTX-Toolkit v0.0.14. Using information
562 from unique molecule identifiers (UMIs) added during library preparation, reads with the same

563 sequence (including UMIs) were collapsed to remove putative PCR duplicates using a custom script.
564 Prior to mapping, UMIs were trimmed (seqtk trimfq -b 4 -e 4) and reads shorter than 15 nucleotides
565 (nts) were discarded (seqtk seq -L 15). Library quality was assessed with FastQC twice, for the raw
566 and for the processed reads. Processed reads were aligned against the *C. elegans* genome assembly
567 WBcel235 with bowtie v0.12.8 (64) (–tryhard –best –strata -v 0 -M 1). Reads mapping to structural
568 genes were filtered out (r/t/s/sn/snoRNA) using Bedtools 2.25.0 (65) (bedtools intersect -v -s -f 0.9)
569 and further analysis was performed using non-structural RNAs.

570 *Small RNA class definition and quantification.* Gene annotation was retrieved from Ensembl
571 (release-38). Transposon coordinates were retrieved from wormbase (PRJNA13758.WS264) and
572 added to the ensembl gene annotation to create a custom annotation used for further analysis. To
573 define RNAs as belonging to particular classes of small RNA, mapped reads were categorized as
574 follows: 21U-RNAs (piRNAs) are considered those sequences that are 21 nt long, and map sense to
575 annotated piRNA loci; 22G-RNAs are those whose sequence is exactly 20-23 nts, have a guanine at
576 their 5' and map antisense to annotated protein-coding/pseudogenes/lincRNA/transposons; 26G-
577 RNAs, are those which are 26 nt, and map antisense to annotated protein-
578 coding/pseudogenes/lincRNA. Read filtering was done with a python script available at
579 https://github.com/adomingues/filterReads/blob/master/filterReads/filterSmallRNAclasses.py which
580 relies on pysam v0.8.1 an htslib wrapper (66), in combination with Bedtools intersect. Reads fulfilling
581 these definitions were then counted for each library (total levels). Genome browser tracks were
582 created using Bedtools (genomeCoverageBed -bg -split -scale -ibam -g), to summarize genome
583 coverage normalized to mapped reads * 1 million (Reads Per Million or RPM), followed by
584 bedGraphToBigWig to create the bigwig track. To quantify the effects on small RNAs of particular
585 branches/pathways, we collected lists of genes previously identified as being targeted by these
586 pathways: CSR-1 (36); NRDE-3 (43); Mutators (67); and WAGO-1 (52). ERGO-1 targets were defined
587 as genes that lose oxidation-resistant 26G-RNAs (that are 3' 2'-O-methylated) upon *gtsf-1* mutation
588 (Table EV1, sheet 1.2 in reference 32). ALG-3/4 targets are defined as genes that lose 26G-RNAs upon

589 *gtsf-1* mutation (Table EV1, sheet 1.1 in reference 32), excluding ERGO-1 targets. The genomic
590 locations of 22G- and 26G-RNAs was then intersected with that of the genes, and counted for each
591 library.

592 *mRNA read processing and mapping.* library quality was assessed with FastQC before being
593 aligned against the *C. elegans* genome assembly WBcel235 and a custom GTF, which included
594 transposon coordinates (described above) with STAR v2.5.2b (–runMode alignReads –
595 outSAMattributes Standard –outSJfilterReads Unique –outSAMunmapped Within –
596 outReadsUnmapped None –outFilterMismatchNmax 2 –outFilterMultimapNmax 10 –alignIntronMin
597 21 –sjdbOverhang 79). Reads mapping to annotated features in the custom GTF were counted with
598 subread featureCounts v1.5.1 (-s 2 -p -F GTF –donotsort -t exon -g gene_id). Coverage tracks were
599 generated with deepTools v2.4.3 (bamCoverage –smoothLength 60 –binSize 20 –
600 normalizeUsingRPKM) (68).

601 *Differential expression/small RNA targeting.* Reads mapping to annotated features in the
602 custom GTF were counted with htseq-count v0.9.0 (69)(htseq-count -f bam -m intersection-
603 nonempty -s reverse) for sRNA-seq data, and with subread featureCounts v1.5.1 (70) (-s 2 -p -F GTF –
604 donotsort -t exon -g gene_id) for mRNA-seq. Pairwise differential expression comparisons were
605 performed with DESeq2 v.1.18.1 (71). For the selection of genes differentially targeted (sRNA) or
606 expressed (mRNA), a further cut-off of at least a 1.5 fold-change difference between conditions was
607 applied. As previously reported (32), due to the observed global depletion of 26G-RNA reads in some
608 samples (sRNA), DESeq2 library sizes computed from all reads 18-30 nt in each sample were for 26G-
609 RNA differential analyses. Gene expression in RPKM (Reads Per Kilobase Million) was calculated by
610 retrieving the fragments/counts per million mapped fragments from the DEseq2 object (fpm(object,
611 robust = TRUE)) and normalizing to gene length.

612 *Metagene analysis.* The average coverage at each gene from a particular branch was
613 determined with deepTools v2.4.3 (computeMatrix scale-regions –metagene –missingDataAsZero –b

614 250 -a 250 –regionBodyLength 2000 –binSize 50 –averageTypeBins median), using the transcript
615 locations of each gene, and plotted with plotProfile –plotType se –averageType mean –perGroup.

616 *UTR targeting by 26G-RNAs*. To identify genes predominantly targeted at their 5' or 3',
617 coverage values of scaled genes were obtained with deepTools, as done for the metagene analysis
618 (see above), with the difference that only the WT track was used, and options -a and -b were set to
619 0. That is, only the scaled body regions were used. 5' and 3' sRNA targeting was defined for each
620 gene based on the coverage at the first or last 25% of the scaled gene body. The genes were then
621 classified in low, medium or high targeting if they were in the 0-25, 25-75, or 75-100 percentile of the
622 sRNA coverage distribution for either the 5' or the 3'. Primarily 5' or 3' targeted genes were further
623 defined if they were in the 5' high and 3' low category (5' targeted), or high in the 3' and low in the 5'
624 (3' targeted).

625

626 **Accession numbers**

627 All sequencing data has been submitted to SRA, accession number PRJNA497368.

628

629 **Author Contributions**

630 Conceptualization, M.V.A. and R.F.K.; Investigation, M.V.A.; Formal Analysis, M.V.A.,
631 A.M.dJ.D.; Visualization, M.V.A., A.M.dJ.D.; Writing – Original Draft, all authors contributed; Writing –
632 Review & Editing, all authors contributed; Funding acquisition, R.F.K.

633

634 **Competing Interests**

635 The authors declare that they have no conflict of interest.

636

637 **Acknowledgements**

We thank all the members of the Ketting lab for great help and discussion. A special thanks to Yasmin el Sherif and Svenja Hellmann for excellent technical assistance and to Jan Schreier for producing the *mut-16(xf142)* mutant. The authors are grateful to Hanna Lukas, Clara Werner and Maria Mendez-Lago of the IMB genomics core facility for library preparation. We thank the IMB Media Lab for consumables. We also acknowledge the *Caenorhabditis* Genetics Center (CGC), which is funded by NIH Office of Research Infrastructure Programs (P40 OD010440), for providing worm strains. This work was supported by a Deutsche Forschungsgemeinschaft grant KE 1888/1-1 (Project Funding Programme to R.F.K.).

646 **References**

647 1. Ha M, Kim VN. Regulation of microRNA biogenesis. Nat Rev Mol Cell Biol. 2014 Aug;15(8):509–
648 24.

649 2. Ernst C, Odom DT, Kutter C. The emergence of piRNAs against transposon invasion to preserve
650 mammalian genome integrity. Nat Commun. 2017 Nov 10;8(1):1411.

651 3. Huang X, Fejes Tóth K, Aravin AA. piRNA Biogenesis in Drosophila melanogaster. Trends Genet.
652 2017 Nov 1;33(11):882–94.

653 4. Luteijn MJ, Ketting RF. PIWI-interacting RNAs: from generation to transgenerational
654 epigenetics. Nat Rev Genet. 2013 Aug;14(8):523–34.

655 5. Rojas-Ríos P, Simonelig M. piRNAs and PIWI proteins: regulators of gene expression in
656 development and stem cells. Development. 2018 Sep 1;145(17):dev161786.

657 6. Borges F, Martienssen RA. The expanding world of small RNAs in plants. Nat Rev Mol Cell Biol.
658 2015 Dec;16(12):727–41.

659 7. Holoch D, Moazed D. RNA-mediated epigenetic regulation of gene expression. Nat Rev Genet.
660 2015 Feb;16(2):71–84.

661 8. Kim VN, Han J, Siomi MC. Biogenesis of small RNAs in animals. Nat Rev Mol Cell Biol. 2009
662 Feb;10(2):126–39.

663 9. Malone CD, Hannon GJ. Small RNAs as Guardians of the Genome. Cell. 2009 Feb 20;136(4):656–
664 68.

665 10. Akkouche A, Grentzinger T, Fablet M, Armenise C, Burlet N, Braman V, et al. Maternally
666 deposited germline piRNAs silence the tirant retrotransposon in somatic cells. EMBO Rep. 2013
667 May 1;14(5):458–64.

668 11. Brennecke J, Aravin AA, Stark A, Dus M, Kellis M, Sachidanandam R, et al. Discrete Small RNA-
669 Generating Loci as Master Regulators of Transposon Activity in Drosophila. Cell. 2007 Mar
670 23;128(6):1089–103.

671 12. Brennecke J, Malone CD, Aravin AA, Sachidanandam R, Stark A, Hannon GJ. An Epigenetic Role
672 for Maternally Inherited piRNAs in Transposon Silencing. Science. 2008 Nov
673 28;322(5906):1387–92.

674 13. de Albuquerque BFM, Placentino M, Ketting RF. Maternal piRNAs Are Essential for Germline
675 Development following De Novo Establishment of Endo-siRNAs in Caenorhabditis elegans. Dev
676 Cell. 2015 Aug 24;34(4):448–56.

677 14. Houwing S, Kamminga LM, Berezikov E, Cronembold D, Girard A, van den Elst H, et al. A Role for
678 Piwi and piRNAs in Germ Cell Maintenance and Transposon Silencing in Zebrafish. Cell. 2007
679 Apr 6;129(1):69–82.

680 15. Le Thomas A, Stuwe E, Li S, Du J, Marinov G, Rozhkov N, et al. Transgenerationally inherited
681 piRNAs trigger piRNA biogenesis by changing the chromatin of piRNA clusters and inducing
682 precursor processing. Genes Dev. 2014 Jan 8;28(15):1667–80.

683 16. Martinez G, Köhler C. Role of small RNAs in epigenetic reprogramming during plant sexual
684 reproduction. Curr Opin Plant Biol. 2017 Apr 1;36:22–8.

685 17. Czech B, Malone CD, Zhou R, Stark A, Schlingeheyde C, Dus M, et al. An endogenous small
686 interfering RNA pathway in *Drosophila*. Nature. 2008 Jun;453(7196):798–802.

687 18. Tam OH, Aravin AA, Stein P, Girard A, Murchison EP, Cheloufi S, et al. Pseudogene-derived small
688 interfering RNAs regulate gene expression in mouse oocytes. Nature. 2008
689 May;453(7194):534–8.

690 19. Watanabe T, Totoki Y, Toyoda A, Kaneda M, Kuramochi-Miyagawa S, Obata Y, et al. Endogenous
691 siRNAs from naturally formed dsRNAs regulate transcripts in mouse oocytes. Nature. 2008
692 May;453(7194):539–43.

693 20. Fire A, Xu S, Montgomery MK, Kostas SA, Driver SE, Mello CC. Potent and specific genetic
694 interference by double-stranded RNA in Caenorhabditis elegans. Nature. 1998 Feb
695 19;391(6669):806–11.

696 21. Yigit E, Batista PJ, Bei Y, Pang KM, Chen C-CG, Tolia NH, et al. Analysis of the C. elegans
697 Argonaute Family Reveals that Distinct Argonautes Act Sequentially during RNAi. Cell. 2006 Nov
698 17;127(4):747–57.

699 22. Ambros V, Lee RC, Lavanway A, Williams PT, Jewell D. MicroRNAs and Other Tiny Endogenous
700 RNAs in C. elegans. Curr Biol. 2003 May 13;13(10):807–18.

701 23. Ruby JG, Jan C, Player C, Axtell MJ, Lee W, Nusbaum C, et al. Large-Scale Sequencing Reveals
702 21U-RNAs and Additional MicroRNAs and Endogenous siRNAs in C. elegans. Cell. 2006 Dec
703 15;127(6):1193–207.

704 24. Batista PJ, Ruby JG, Claycomb JM, Chiang R, Fahlgren N, Kasschau KD, et al. PRG-1 and 21U-
705 RNAs Interact to Form the piRNA Complex Required for Fertility in C. elegans. Mol Cell. 2008 Jul
706 11;31(1):67–78.

707 25. Das PP, Bagijn MP, Goldstein LD, Woolford JR, Lehrbach NJ, Sapetschnig A, et al. Piwi and
708 piRNAs Act Upstream of an Endogenous siRNA Pathway to Suppress Tc3 Transposon Mobility in
709 the Caenorhabditis elegans Germline. Mol Cell. 2008 Jul 11;31(1):79–90.

710 26. Wang G, Reinke V. A C. elegans Piwi, PRG-1, Regulates 21U-RNAs during Spermatogenesis. Curr
711 Biol. 2008 Jun 24;18(12):861–7.

712 27. Conine CC, Batista PJ, Gu W, Claycomb JM, Chaves DA, Shirayama M, et al. Argonautes ALG-3
713 and ALG-4 are required for spermatogenesis-specific 26G-RNAs and thermotolerant sperm in
714 Caenorhabditis elegans. Proc Natl Acad Sci U S A. 2010;107(8):3588–3593.

715 28. Gent JI, Lamm AT, Pavelec DM, Maniar JM, Parameswaran P, Tao L, et al. Distinct Phases of
716 siRNA Synthesis in an Endogenous RNAi Pathway in C. elegans Soma. Mol Cell. 2010 Mar
717 12;37(5):679–89.

718 29. Vasale JJ, Gu W, Thivierge C, Batista PJ, Claycomb JM, Youngman EM, et al. Sequential rounds of
719 RNA-dependent RNA transcription drive endogenous small-RNA biogenesis in the ERGO-
720 1/Argonaute pathway. Proc Natl Acad Sci. 2010 Feb 23;107(8):3582–7.

721 30. Gent JI, Schvarzstein M, Villeneuve AM, Gu SG, Jantsch V, Fire AZ, et al. A Caenorhabditis
722 elegans RNA-Directed RNA Polymerase in Sperm Development and Endogenous RNA
723 Interference. Genetics. 2009 Jan 12;183(4):1297–314.

724 31. Han T, Manoharan AP, Harkins TT, Bouffard P, Fitzpatrick C, Chu DS, et al. 26G endo-siRNAs
725 regulate spermatogenic and zygotic gene expression in Caenorhabditis elegans. Proc Natl Acad
726 Sci. 2009 Mar 11;106(44):18674–9.

727 32. Almeida MV, Dietz S, Redl S, Karaulanov E, Hildebrandt A, Renz C, et al. GTSF-1 is required for
728 formation of a functional RNA-dependent RNA Polymerase complex in Caenorhabditis elegans.
729 EMBO J. 2018 Jun 15;37(12):e99325.

730 33. Duchaine TF, Wohlschlegel JA, Kennedy S, Bei Y, Conte Jr. D, Pang K, et al. Functional
731 Proteomics Reveals the Biochemical Niche of C. elegans DCR-1 in Multiple Small-RNA-Mediated
732 Pathways. Cell. 2006 Jan 27;124(2):343–54.

733 34. Pavelec DM, Lachowiec J, Duchaine TF, Smith HE, Kennedy S. Requirement for the ERI/DICER
734 Complex in Endogenous RNA Interference and Sperm Development in Caenorhabditis elegans.
735 Genetics. 2009 Dec 1;183(4):1283–95.

736 35. Thivierge C, Makil N, Flamand M, Vasale JJ, Mello CC, Wohlschlegel J, et al. Tudor domain ERI-5
737 tethers an RNA-dependent RNA polymerase to DCR-1 to potentiate endo-RNAi. Nat Struct Mol
738 Biol. 2012 Jan;19(1):90–7.

739 36. Conine CC, Moresco JJ, Gu W, Shirayama M, Conte D, Yates JR, et al. Argonautes promote male
740 fertility and provide a paternal memory of germline gene expression in C. Elegans. Cell.
741 2013;155(7):1532–1544.

742 37. Billi AC, Alessi AF, Khivansara V, Han T, Freeberg M, Mitani S, et al. The Caenorhabditis elegans
743 HEN1 Ortholog, HENN-1, Methylates and Stabilizes Select Subclasses of Germline Small RNAs.
744 PLoS Genet. 2012 Apr 19;8(4):e1002617.

745 38. Kamminga LM, van Wolfswinkel JC, Luteijn MJ, Kaaij LJT, Bagijn MP, Sapetschnig A, et al.
746 Differential Impact of the HEN1 Homolog HENN-1 on 21U and 26G RNAs in the Germline of
747 Caenorhabditis elegans. PLoS Genet. 2012 Jul 19;8(7):e1002702.

748 39. Montgomery TA, Rim Y-S, Zhang C, Dowen RH, Phillips CM, Fischer SEJ, et al. PIWI Associated
749 siRNAs and piRNAs Specifically Require the Caenorhabditis elegans HEN1 Ortholog henn-1. PLoS
750 Genet. 2012 Apr 19;8(4):e1002616.

751 40. Fischer SEJ, Montgomery T a., Zhang C, Fahlgren N, Breen PC, Hwang A, et al. The ERI-6/7
752 helicase acts at the first stage of an siRNA amplification pathway that targets recent gene
753 duplications. PLoS Genet. 2011;7(11).

754 41. Newman MA, Ji F, Fischer SEJ, Anselmo A, Sadreyev RI, Ruvkun G. The surveillance of pre-mRNA
755 splicing is an early step in C. elegans RNAi of endogenous genes. Genes Dev [Internet]. 2018
756 May 8 [cited 2018 May 14]; Available from:
757 http://genesdev.cshlp.org/content/early/2018/05/08/gad.311514.118

758 42. Guang S, Bochner AF, Pavelec DM, Burkhart KB, Harding S, Lachowiec J, et al. An Argonaute
759 Transports siRNAs from the Cytoplasm to the Nucleus. Science. 2008 Jul 25;321(5888):537–41.

760 43. Zhou X, Xu F, Mao H, Ji J, Yin M, Feng X, et al. Nuclear RNAi Contributes to the Silencing of Off-
761 Target Genes and Repetitive Sequences in Caenorhabditis elegans. Genetics. 2014 May
762 1;197(1):121–32.

763 44. Lee RC, Hammell CM, Ambros V. Interacting endogenous and exogenous RNAi pathways in
764 Caenorhabditis elegans. RNA. 2006 Jan 4;12(4):589–97.

765 45. Zhuang JJ, Hunter CP. Tissue-specificity of Caenorhabditis elegans Enhanced RNAi Mutants.
766 Genetics. 2011 Jan 1;genetics.111.127209.

767 46. Phillips CM, Montgomery TA, Breen PC, Ruvkun G. MUT-16 promotes formation of perinuclear
768 Mutator foci required for RNA silencing in the C. elegans germline. Genes Dev. 2012 Jan
769 7;26(13):1433–44.

770 47. Almeida MVV, Domingues AM de J, Lukas H, Mendez-Lago M, Ketting RF. RppH can faithfully
771 replace TAP to allow cloning of 5'-triphosphate carrying small RNAs. bioRxiv. 2018 Mar
772 21;283077.

773 48. Claycomb JM, Batista PJ, Pang KM, Gu W, Vasale JJ, van Wolfswinkel JC, et al. The Argonaute
774 CSR-1 and Its 22G-RNA Cofactors Are Required for Holocentric Chromosome Segregation. Cell.
775 2009 Oct 2;139(1):123–34.

776 49. Luteijn MJ, van Bergeijk P, Kaaij LJT, Almeida MV, Roovers EF, Berezikov E, et al. Extremely
777 stable Piwi-induced gene silencing in Caenorhabditis elegans. EMBO J. 2012 Aug
778 15;31(16):3422–30.

779 50. Stoeckius M, Grün D, Rajewsky N. Paternal RNA contributions in the Caenorhabditis elegans
780 zygote. EMBO J. 2014 Aug 18;33(16):1740–50.

781 51. Stoeckius M, Maaskola J, Colombo T, Rahn H-P, Friedländer MR, Li N, et al. Large-scale sorting
782 of *C. elegans* embryos reveals the dynamics of small RNA expression. Nat Methods. 2009
783 Oct;6(10):745–51.

784 52. Gu W, Shirayama M, Conte Jr. D, Vasale J, Batista PJ, Claycomb JM, et al. Distinct Argonaute-
785 Mediated 22G-RNA Pathways Direct Genome Surveillance in the C. elegans Germline. Mol Cell.
786 2009 Oct 23;36(2):231–44.

787 53. Minkina O, Hunter CP. Stable Heritable Germline Silencing Directs Somatic Silencing at an
788 Endogenous Locus. Mol Cell. 2017 Feb 16;65(4):659-670.e5.

789 54. Schott D, Yanai I, Hunter CP. Natural RNA interference directs a heritable response to the
790 environment. Sci Rep. 2014 Dec 9;4:7387.

791 55. Wan G, Fields BD, Spracklin G, Shukla A, Phillips CM, Kennedy S. Spatiotemporal regulation of
792 liquid-like condensates in epigenetic inheritance. Nature. 2018 May 16;1.

793 56. Xu F, Feng X, Chen X, Weng C, Yan Q, Xu T, et al. A Cytoplasmic Argonaute Protein Promotes the
794 Inheritance of RNAi. Cell Rep. 2018 May 22;23(8):2482–94.

795 57. Shirayama M, Seth M, Lee H-C, Gu W, Ishidate T, Conte Jr. D, et al. piRNAs Initiate an Epigenetic
796 Memory of Nonself RNA in the C. elegans Germline. Cell. 2012 Jul 6;150(1):65–77.

797 58. Ashe A, Sapetschnig A, Weick E-M, Mitchell J, Bagijn MP, Cording AC, et al. piRNAs Can Trigger a
798 Multigenerational Epigenetic Memory in the Germline of C. elegans. Cell. 2012 Jul 6;150(1):88–
799 99.

800 59. Houri-Ze'evi L, Korem Y, Sheftel H, Faigenbloom L, Toker IA, Dagan Y, et al. A Tunable
801 Mechanism Determines the Duration of the Transgenerational Small RNA Inheritance in
802 C. elegans. Cell. 2016 Mar 24;165(1):88–99.

803 60. Ghildiyal M, Seitz H, Horwich MD, Li C, Du T, Lee S, et al. Endogenous siRNAs Derived from
804 Transposons and mRNAs in Drosophila Somatic Cells. Science. 2008 May 23;320(5879):1077–
805 81.

806 61. Brenner S. The Genetics of Caenorhabditis Elegans. Genetics. 1974 Jan 5;77(1):71–94.

807 62. Kamath RS, Fraser AG, Dong Y, Poulin G, Durbin R, Gotta M, et al. Systematic functional analysis
808 of the Caenorhabditis elegans genome using RNAi. Nature. 2003 Jan 16;421(6920):231–7.

809 63. Martin M. Cutadapt removes adapter sequences from high-throughput sequencing reads.
810 EMBnet.journal. 2011 May 2;17(1):10–2.

811 64. Langmead B, Trapnell C, Pop M, Salzberg SL. Ultrafast and memory-efficient alignment of short
812 DNA sequences to the human genome. Genome Biol. 2009 Mar 4;10:R25.

813 65. Quinlan AR, Hall IM. BEDTools: a flexible suite of utilities for comparing genomic features.
814 Bioinformatics. 2010 Mar 15;26(6):841–2.

66. Li H, Handsaker B, Wysoker A, Fennell T, Ruan J, Homer N, et al. The Sequence Alignment/Map format and SAMtools. Bioinformatics. 2009 Aug 15;25(16):2078–9.

67. Phillips CM, Montgomery BE, Breen PC, Roovers EF, Rim Y-S, Ohsumi TK, et al. MUT-14 and SMUT-1 DEAD Box RNA Helicases Have Overlapping Roles in Germline RNAi and Endogenous siRNA Formation. Curr Biol. 2014 Apr 14;24(8):839–44.

68. Ramírez F, Ryan DP, Grüning B, Bhardwaj V, Kilpert F, Richter AS, et al. deepTools2: a next generation web server for deep-sequencing data analysis. Nucleic Acids Res. 2016 Jul 8;44(W1):W160–5.

69. Anders S, Pyl PT, Huber W. HTSeq—a Python framework to work with high-throughput sequencing data. Bioinformatics. 2014 Sep;btu638.

70. Liao Y, Smyth GK, Shi W. featureCounts: an efficient general purpose program for assigning sequence reads to genomic features. Bioinformatics. 2014 Apr 1;30(7):923–30.

71. Love MI, Huber W, Anders S. Moderated estimation of fold change and dispersion for RNA-seq data with DESeq2. Genome Biol [Internet]. 2014 Dec [cited 2016 Jul 28];15(12). Available from: http://genomebiology.biomedcentral.com/articles/10.1186/s13059-014-0550-8

832 **Fig Captions**

833 **Fig 1. Maternal and zygotic sRNAs drive RNAi in the soma.** (A) Experimental setup to address
834 maternal transmission of the Eri phenotype in *gtsf-1* mutants. Eri phenotype was assessed by
835 transferring worms to plates containing *lir-1* RNAi food and scoring for larval arrest. *dpy-4(e1166)* is
836 weakly semi-dominant. Since the phenotype is mild, for simplicity, we will refer to *dpy-4(e1166)*
837 heterozygotes as "wild-type". (B, D-F) Schematics of genetic crosses using the 22G sensor
838 background. Green worms illustrate ubiquitous derepression of 22G sensor. Unless otherwise noted,
839 for all crosses the number of scored F1s, F2s and F3s was each >50. (C) Related to the cross shown in
840 (B). Wide-field fluorescence microscopy images showing 22G sensor GFP signal. Five representative
841 gravid adult hermaphrodites or adult males from each generation are shown. Of note, some
842 autofluorescence of the gut is observed in gravid adult animals, and is especially noticeable in worms
843 with the sensor off. Scale bars represent 0,25 mm.

844

845 **Fig 2. sRNA dynamics in Eri maternal inheritance.** (A) Schematics of the cross setup used to isolate
846 worms of different generations and *gtsf-1* genotypes. *gtsf-1;dpy-4* mutants were outcrossed with N2
847 males, allowed to self for two generations and then WT, Dpy mutant F1 and Dpy mutant F2 young
848 adult animals were isolated, RNA was extracted, sRNAs and mRNAs were cloned and sequenced.
849 sRNA libraries were either prepared directly or after treatment with RppH. WT, wild-type. (B-F, H)
850 Normalized levels of sRNAs, in RPM (Reads Per Million), per generation/phenotype. Four biological
851 replicates are shown. (B) Total levels of 26G-RNAs in the untreated libraries. (C) Total levels of 26G-
852 RNAs mapping to ERGO-1 targets in the untreated libraries. (D) Total levels of 26G-RNAs mapping to
853 ALG-3/4 targets in the untreated libraries. (E) Total levels of 22G-RNAs in the RppH-treated libraries.
854 (F) Total levels of 22G-RNAs mapping to ERGO-1 targets in the RppH-treated libraries. (G) Genome
855 browser tracks of the X-cluster, a known set of ERGO-1 targets, showing mapped 26G- and 22G-
856 RNAs. 26G- and 22G-RNA tracks were obtained from untreated and RppH-treated libraries,

857 respectively. (H) Total levels of 22G-RNAs mapping to ALG-3/4 targets in RppH-treated libraries. P-
858 values were calculated with a two-sided unpaired t-test.

859

860 **Fig 3. mRNA dynamics in Eri maternal inheritance.** (A) Genome browser tracks showing mRNA, in
861 RPKM (Reads Per Kilobase Million), of X-cluster genes. (B) Distribution of normalized mRNA
862 expression, in RPKM, of all expressed genes, ALG-3/4 targets and ERGO-1 targets in different
863 generations/phenotype. (C) Distribution of normalized mRNA expression, in RPKM, of all expressed
864 genes (upper panel), ALG-3/4 targets (middle panel) and ERGO-1 targets (lower panel) throughout
865 development. Expression is shown for wild-type N2 (in blue) and *rrf-3(pk1426)* (in red) animals. YA,
866 young adult. L1-L4, first to fourth larval stages of *C. elegans* development. Violin plots in (B-C) show
867 the distribution density of the underlying data. The top and bottom of the embedded box represent
868 the 75th and the 25th percentile of the distribution, respectively. The line in the box represents the
869 median. P-values were calculated with a two-sided unpaired Mann-Whitney/Wilcoxon rank-sum test.

870

871 **Fig 4. GTSF-1 is required for sRNA biogenesis and target silencing in adult males.** (A-E) Normalized
872 levels of sRNAs in RppH treated libraries, in RPM. Three biological replicates are shown. WT, wild-
873 type. (A) Total levels of 26G-RNAs. (B) 26G-RNAs mapping to ERGO-1 targets. (C) 26G-RNAs mapping
874 to ALG-3/4 targets. (D) total levels of 21U-RNAs. (E) total levels of 22G-RNAs. (F) RPM Levels of sRNAs
875 mapping, per gene, to known targets of ALG-3/4 and ERGO-1. (G) Normalized mRNA expression of
876 ALG-3/4 and ERGO-1 targets, in RPKM. Violin plots in (F-G) show the distribution density of the
877 underlying data. The top and bottom of the embedded box represent the 75th and the 25th
878 percentile of the distribution, respectively. The line in the box represents the median. P-values were
879 calculated either with a two-sided unpaired t-test (A-E), or with a two-sided Mann-
880 Whitney/Wilcoxon rank-sum test (F-G).

881

882 **Fig 5. sRNA abundance is a predictor of regulatory outcome by ALG-3/4.** (A) Distribution of sRNA
883 levels (26G-RNA on the left panel, 22G-RNA on the right panel) mapping to ALG-3/4 targets that are
884 unchanged, down- or upregulated upon *gtsf-1* mutation. (B) MA-plot displaying the 22G-RNA levels
885 in respect to regulatory outcome. (B) is another representation of the data shown in the right panel
886 of (A). Violin plots in (A) show the distribution density of the underlying data. The top and bottom of
887 the embedded box represent the 75th and the 25th percentile of the distribution, respectively. The
888 line in the box represents the median. P-values were calculated with a two-sided unpaired Mann-
889 Whitney/Wilcoxon rank-sum test.

890

891 **Fig 6. Predictors of regulatory outcome by ALG-3/4 in males, and ERGO-1 branch sRNA metagene**
892 **analysis.** (A-B) Metagene analysis of 26G- (left panel) and 22G-RNAs (right panel) mapping to ALG-
893 3/4 targets (n=1258) in male datasets (A), and to ERGO-1 targets (n=104) in young adult datasets (B),
894 from our maternal effect setup (as in **Fig 2A**). Target gene body length was scaled between
895 transcription start site (TSS) and transcription end site (TES). Moreover, the regions comprising 250
896 nucleotides immediately upstream of the TSS and downstream of the TES are also included. (C)
897 Regulation of ALG-3/4 target genes predominantly targeted on the 5' or on the 3' by 26G-RNAs. (D)
898 Wild-type expression levels, in RPKM, of ALG-3/4 target genes predominantly targeted on the 5' on
899 or the 3' by 26G-RNAs. (E) 3' UTR lengths of all the transcript isoforms annotated for ALG-3/4 target
900 genes, according to effect on gene expression. For (C-E) we used male sequencing datasets. Violin
901 plots in (C-D) and the boxplot in (E) show the distribution of the data. The top and bottom of
902 the embedded boxes represent the 75th and the 25th percentile of the distribution, respectively. The
903 line in the box represents the median. P-values were calculated with a two-sided unpaired Mann-
904 Whitney/Wilcoxon rank-sum test.

905

906 **Fig 7. ALG-3 and ALG-4 are engaged in a negative feedback loop in males.** Genome browser tracks
907 showing 26G-RNAs (upper panels) and 22G-RNAs (middle panels) mapping to *alg-3* (left panels) and
908 *alg-4* (right panels), in RPM. Lower panels show the RPKM mRNA levels of *alg-3* (on the left) and *alg-*
909 *4* (on the right). Sequencing datasets of adult males were used. WT, wild-type.

910

911 **Supporting Information Captions**

912 **Fig S1. Parental effects of the 26G-RNA pathway.** (A) Illustration of the current understanding of
913 26G-RNA pathways. 26G-RNAs are produced by RRF-3, assisted by GTSF-1 and other accessory
914 factors. 26G-RNAs can associate with ALG-3/4 in the spermatogenic gonad (ALG-3/4 branch) or with
915 ERGO-1 in oocytes and embryos (ERGO-1 branch). Upon target binding, RdRPs are recruited and
916 synthesize secondary 22G-RNAs. NRDE-3 binds ERGO-1 branch 22G-RNAs, while is downstream of
917 ALG-3/4 branch 26G-RNAs. Other unidentified Argonautes may play a role in these pathways. (B)
918 Schematics of genetic crosses of mutant strains with the 22G sensor. Green worms illustrate
919 derepression of the 22G sensor. "X" corresponds to different mutant alleles that share the same
920 maternal rescue. (C) Experimental setup to address the maternal transmission of the temperature-
921 sensitive sterility phenotype at 25°C. Worms were constantly grown at 20°C until transfer to 25°C to
922 assay sterility. L2-L3 worms were transferred to 25°C.

923

924 **Fig S2. Dynamics of RNA expression upon *gtsf-1* mutation.** (A) Violin plot showing the distribution of
925 22G-RNAs mapping, per gene, to known targets of diverse sRNA pathways. (B) Genome browser
926 tracks of *ssp-16*, a known ALG-3/4 target, showing mapped 26G- and 22G-RNAs. 26G- and 22G-RNA
927 tracks were obtained from untreated and RppH-treated libraries, respectively. (C) Total 21U-RNA
928 levels in different generations/phenotype, in RPM. (D) Distribution of normalized mRNA expression
929 of CSR-1 targets in RPKM. Violin plots in (A) and (D) show the distribution density of the underlying
930 data. The top and bottom of the embedded box represent the 75th and the 25th percentile of the

931 distribution, respectively. The line in the box represents the median. P-values were calculated with a
932 two-sided unpaired Mann-Whitney/Wilcoxon rank-sum test.

933

934 **Fig S3. mRNA dynamics upon *gtsf-1* mutation.** (A) Genome browser tracks displaying *gtsf-1* mRNA
935 levels in RPKM. The *gtsf-1(xf43)* deletion allele is represented below. *gtsf-1* levels in the mutant F1
936 cover the *xf43* deletion sequence, thereby indicating contamination with Dpy worms that
937 recombined a wild-type copy of *gtsf-1*. The mutant F2 was isolated from mutant F1 Dpy whose *gtsf-1*
938 genotype was confirmed. Therefore, as expected, the only observed reads are flanking the *xf43*
939 deletion. (B) Genome browser tracks with the mRNA levels, in RPKM, of *ssp-16*. Upregulation occurs
940 immediately in the F1, indicating no maternal effect.

941

942 **Fig S4. sRNA and mRNA profiles of ERGO-1 and ALG-3/4 targets in males.** (A-B) RPM levels of 26G-
943 RNAs (upper panels) and 22G-RNAs (middle panels) mapping to the X-cluster (A) and *ssp-16* (B).
944 Lower panels show RPKM mRNA levels of these targets. WT, wild-type.

945

946 **Fig S5. Predictors of regulatory outcome by ALG-3/4 in young adults.** (A) Metagene analysis of 26G-
947 (left panel) and 22G-RNAs (right panel) mapping to ALG-3/4 targets in young adult datasets, from our
948 maternal effect setup (as in **Fig 2A**). On the upper part of each panel is the mean coverage profile for
949 sRNA species in every generation. On the lower part of each panel, the heatmaps show the density
950 across individual targets. Target gene body length was scaled between transcription start site (TSS)
951 and transcription end site (TES). Moreover, the regions comprising 250 nucleotides immediately
952 upstream of the TSS and downstream of the TES are also included. Simultaneous 26G-RNA targeting
953 in the 5' and 3' can be observed in some genes. (B) Violin plot depicting the regulation of ALG-3/4
954 target genes predominantly targeted on the 5' or on the 3' by 26G-RNAs. (C) Violin plot showing the
955 wild-type expression levels of ALG-3/4 target genes predominantly targeted on the 5' on or the 3' by

26G-RNAs. (D) 3' UTR lengths of all the transcript isoforms annotated for ALG-3/4 target genes, according to effect on gene expression. All the panels of this Fig were prepared using young adult sequencing datasets from our maternal effect experiments. In B and D, regulatory outcome was defined as differential gene expression between the wild-type and *gtsf-1* mutant F2. For (B-D) we used male sequencing datasets. Violin plots in (B-C) and the boxplot in (D) show the distribution of the data. The top and bottom of the embedded boxes represent the 75th and the 25th percentile of the distribution, respectively. The lines in the boxes represent the median. P-values were calculated with a two-sided unpaired Mann-Whitney/Wilcoxon rank-sum test.

Fig S6. ALG-3 and ALG-4 are engaged in a negative feedback loop in young adults. Genome browser tracks showing 26G-RNAs (upper panels) and 22G-RNAs (middle panels) mapping to *alg-3* (left panels) and *alg-4* (right panels), in RPM. Lower panels show the RPKM mRNA levels of *alg-3* (on the left) and *alg-4* (on the right). Sequencing datasets of young adults from our maternal effect setup were used.

S1 Table. Sequencing statistics.

S2 Table. Strains used in this study.

S3 Table. Specifics of library preparation and sequencing.

Fig 1

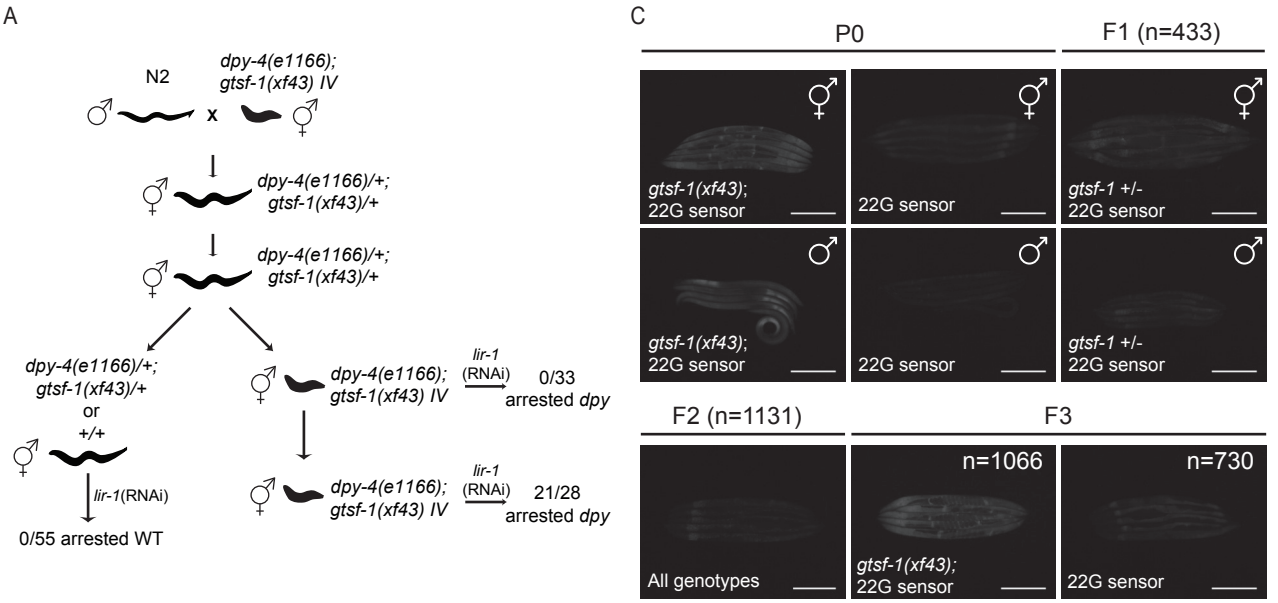

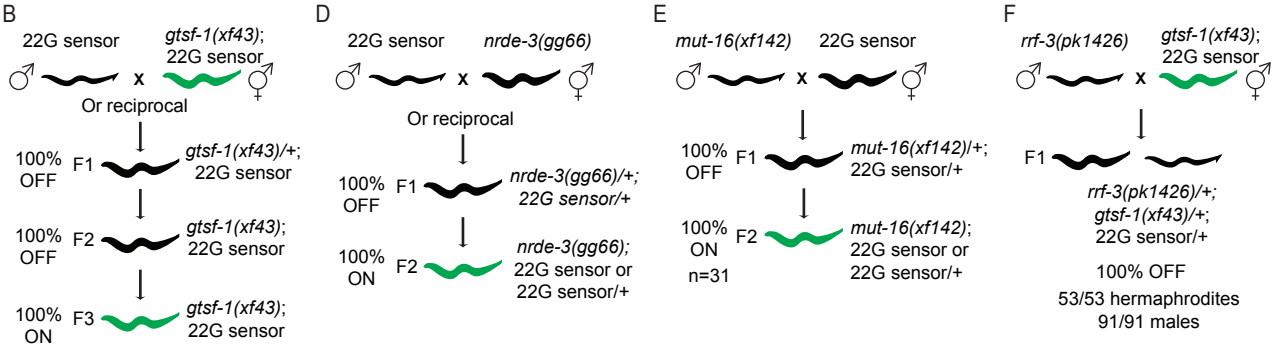

Fig 2

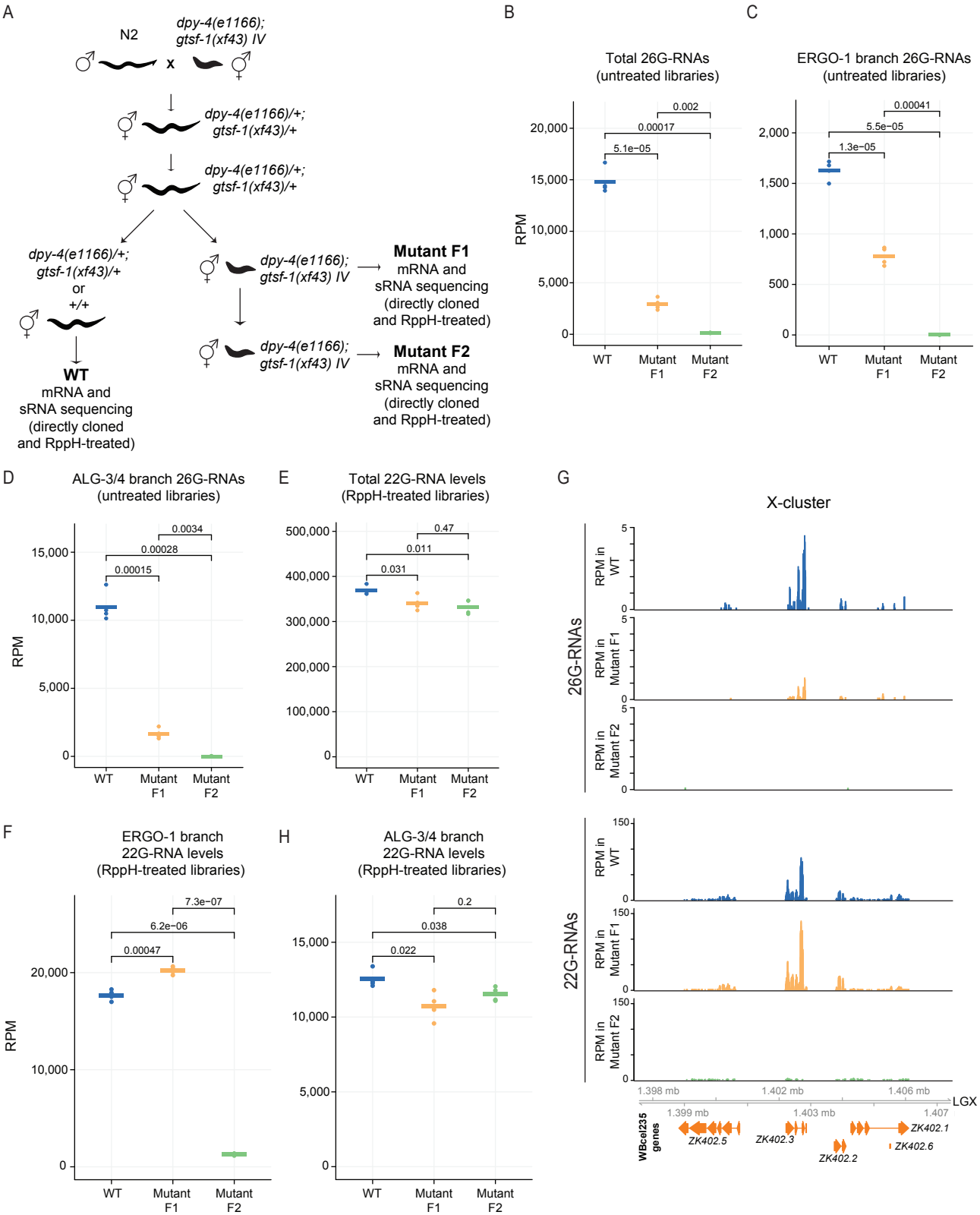

Fig 3

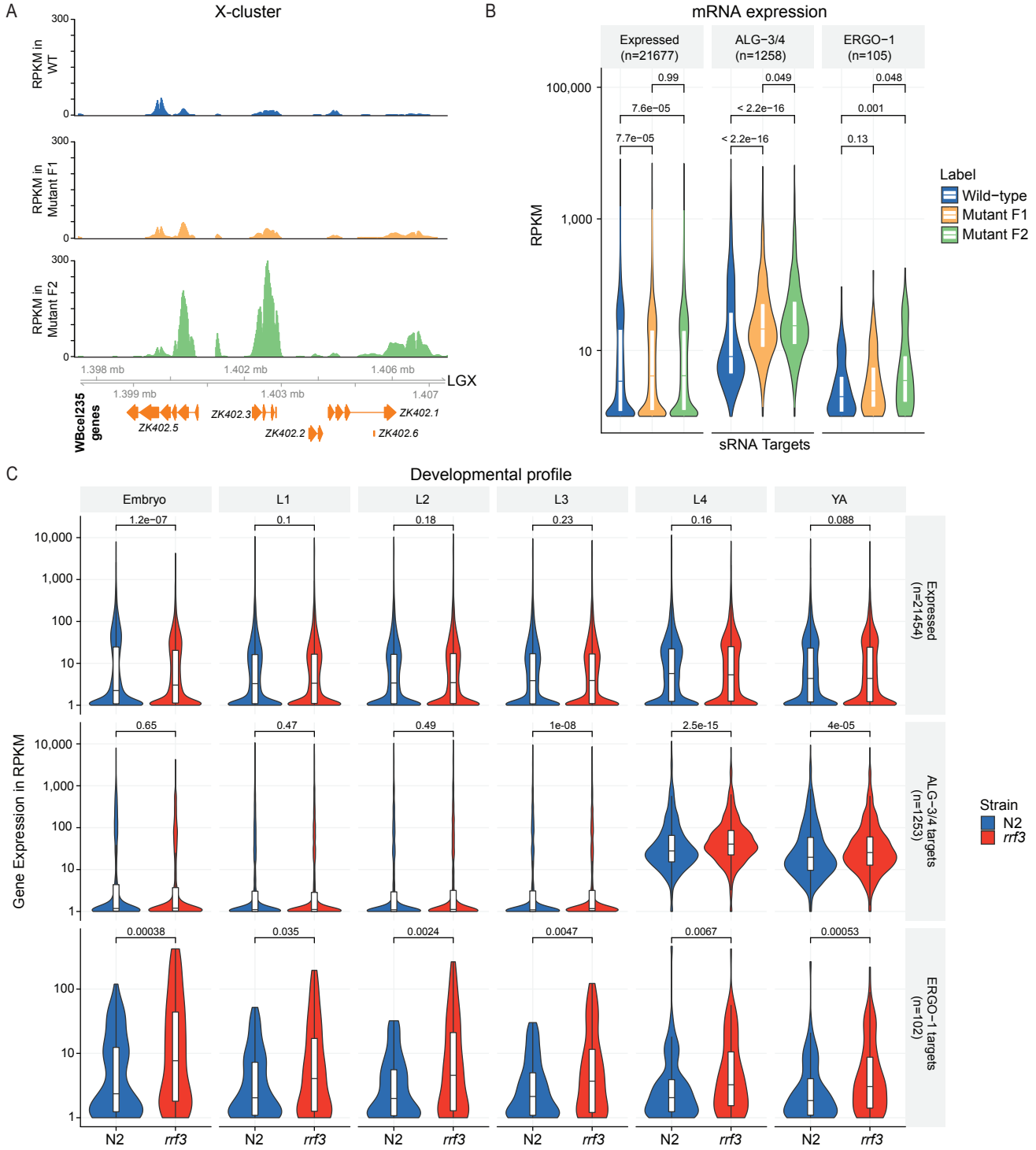
A
X-cluster
RPKM in WT
RPKM in Mutant F1
RPKM in Mutant F2
300
0
1.398 mb
1.402 mb
1.406 mb
LGX
1.399 mb
1.403 mb
1.407
WBcel235 genes
ZK402.5
ZK402.3
ZK402.2
ZK402.1
ZK402.6
B
mRNA expression
Expressed (n=21677)
ALG−3/4 (n=1258)
ERGO−1 (n=105)
RPKM
100,000
1,000
10
0.99
0.049
0.048
7.6e−05
< 2.2e−16
0.001
7.7e−05
< 2.2e−16
0.13
sRNA Targets
Label
Wild−type
Mutant F1
Mutant F2
C
Developmental profile
Embryo
L1
L2
L3
L4
YA
1.2e−07
0.1
0.18
0.23
0.16
0.088
Expressed (n=21454)
0.65
0.47
0.49
1e−08
2.5e−15
4e−05
ALG−3/4 targets (n=1253)
0.00038
0.035
0.0024
0.0047
0.0067
0.00053
ERGO−1 targets (n=102)
Gene Expression in RPKM
10,000
1,000
100
10
1
N2
rrf3
Strain
N2
rrf3

Fig 4

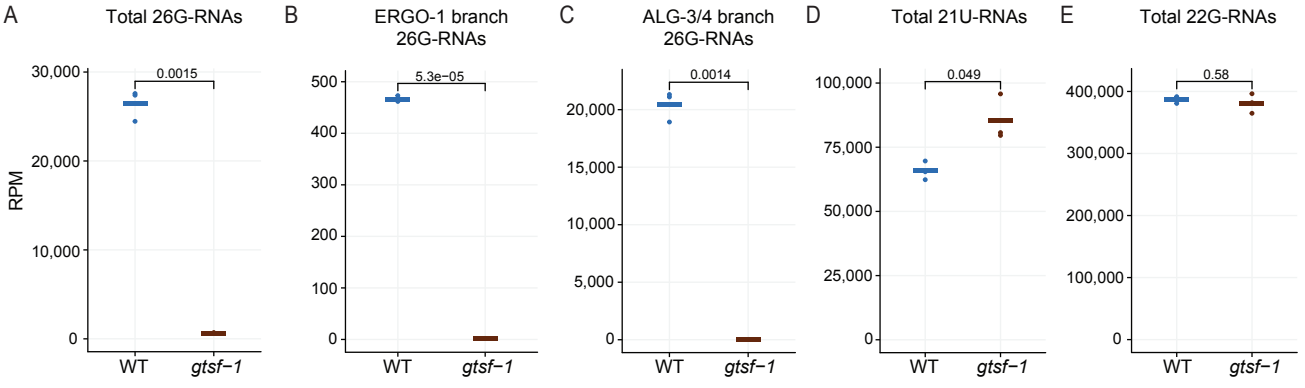
A
Total 26G-RNAs
B
ERGO-1 branch 26G-RNAs
C
ALG-3/4 branch 26G-RNAs
D
Total 21U-RNAs
E
Total 22G-RNAs
RPM
0.0015
5.3e−05
0.0014
0.049
0.58
WT
gtsf−1

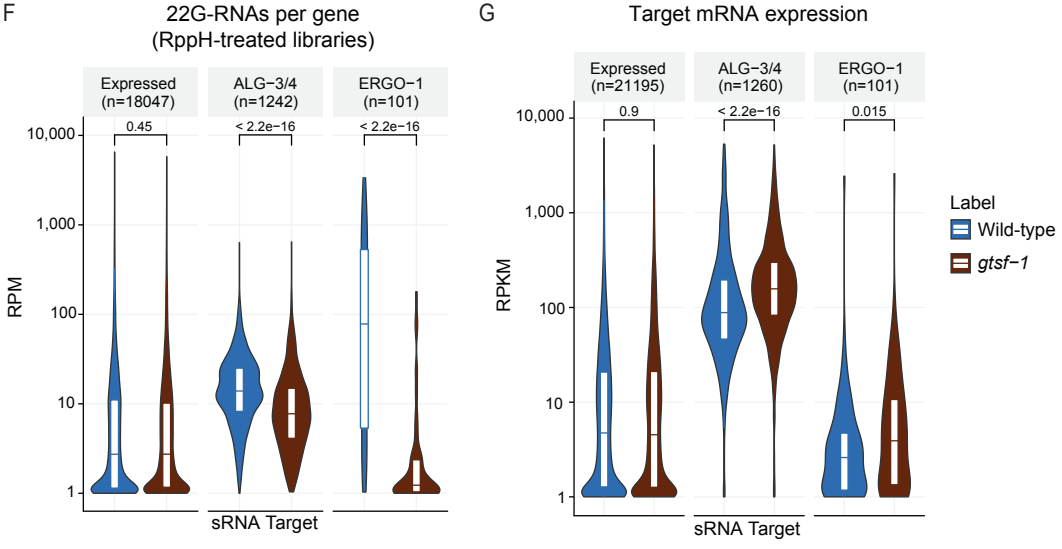
F
22G-RNAs per gene (RppH-treated libraries)
Expressed (n=18047)
ALG−3/4 (n=1242)
ERGO−1 (n=101)
0.45
< 2.2e−16
< 2.2e−16
RPM
sRNA Target
G
Target mRNA expression
Expressed (n=21195)
ALG−3/4 (n=1260)
ERGO−1 (n=101)
0.9
< 2.2e−16
0.015
RPKM
sRNA Target
Label
Wild-type
gtsf−1

Fig. 5

A

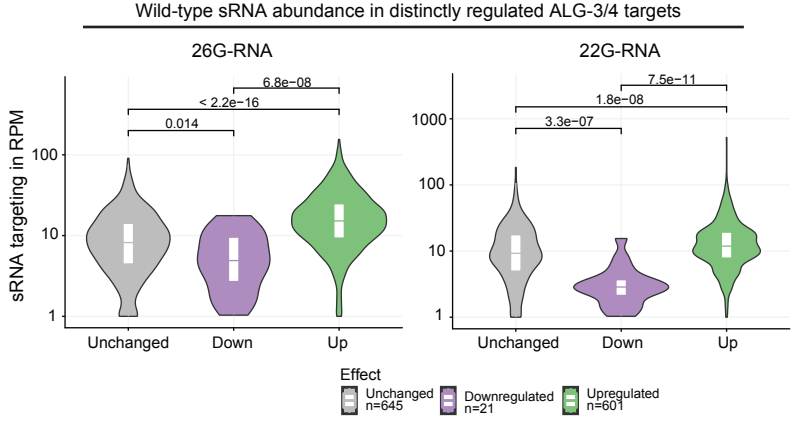
Wild-type sRNA abundance in distinctly regulated ALG-3/4 targets
26G-RNA
22G-RNA
sRNA targeting in RPM
6.8e−08
< 2.2e−16
0.014
7.5e−11
1.8e−08
3.3e−07
100
10
1
1000
Unchanged
Down
Up
Effect
Unchanged n=645
Downregulated n=21
Upregulated n=601

B


ALG-3/4 targets
gtsf-1 vs wild-type males
mRNA fold change (log2)
22G-RNA targeting in RPM
Effect
Unchanged n=645
Downregulated n=21
Upregulated n=601
3
2
1
0
−1
1
10
100

Fig 6

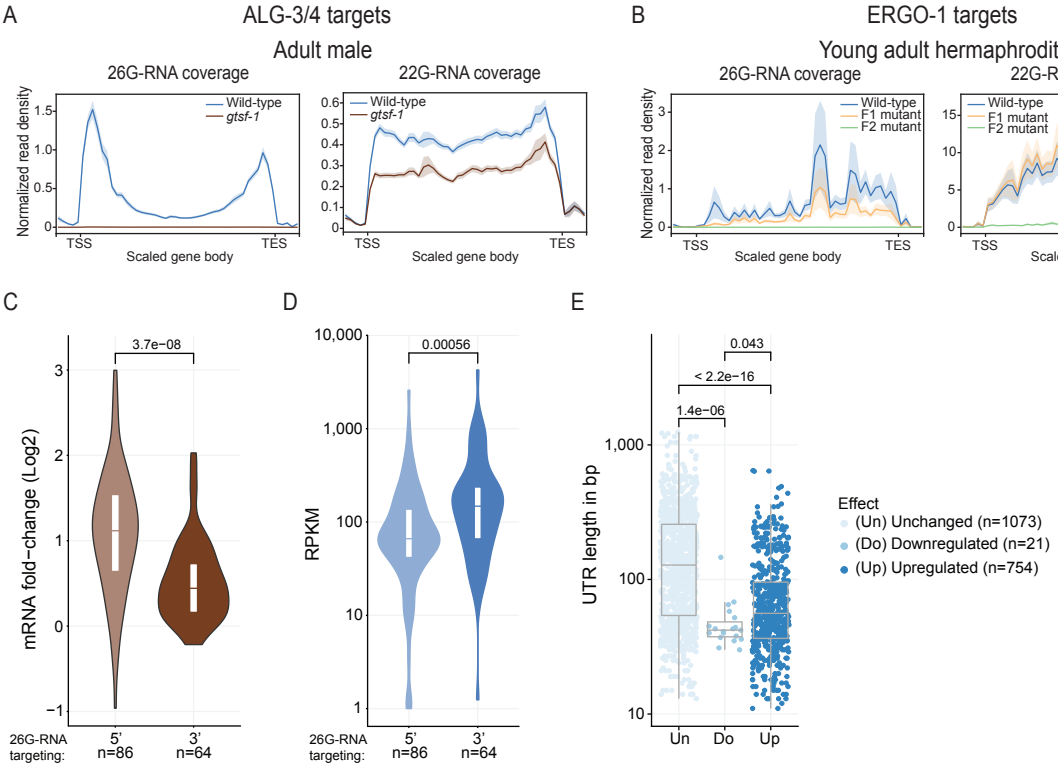
A
ALG-3/4 targets
Adult male
26G-RNA coverage
22G-RNA coverage
Normalized read density
Wild-type
gtsf-1
TSS
TES
Scaled gene body
B
ERGO-1 targets
Young adult hermaphrodite
26G-RNA coverage
22G-RNA coverage
Wild-type
F1 mutant
F2 mutant
C
3.7e−08
mRNA fold−change (Log2)
26G-RNA targeting:
5' n=86
3' n=64
D
0.00056
RPKM
E
0.043
< 2.2e−16
1.4e−06
UTR length in bp
Un
Do
Up
Effect
(Un) Unchanged (n=1073)
(Do) Downregulated (n=21)
(Up) Upregulated (n=754)

Fig 7

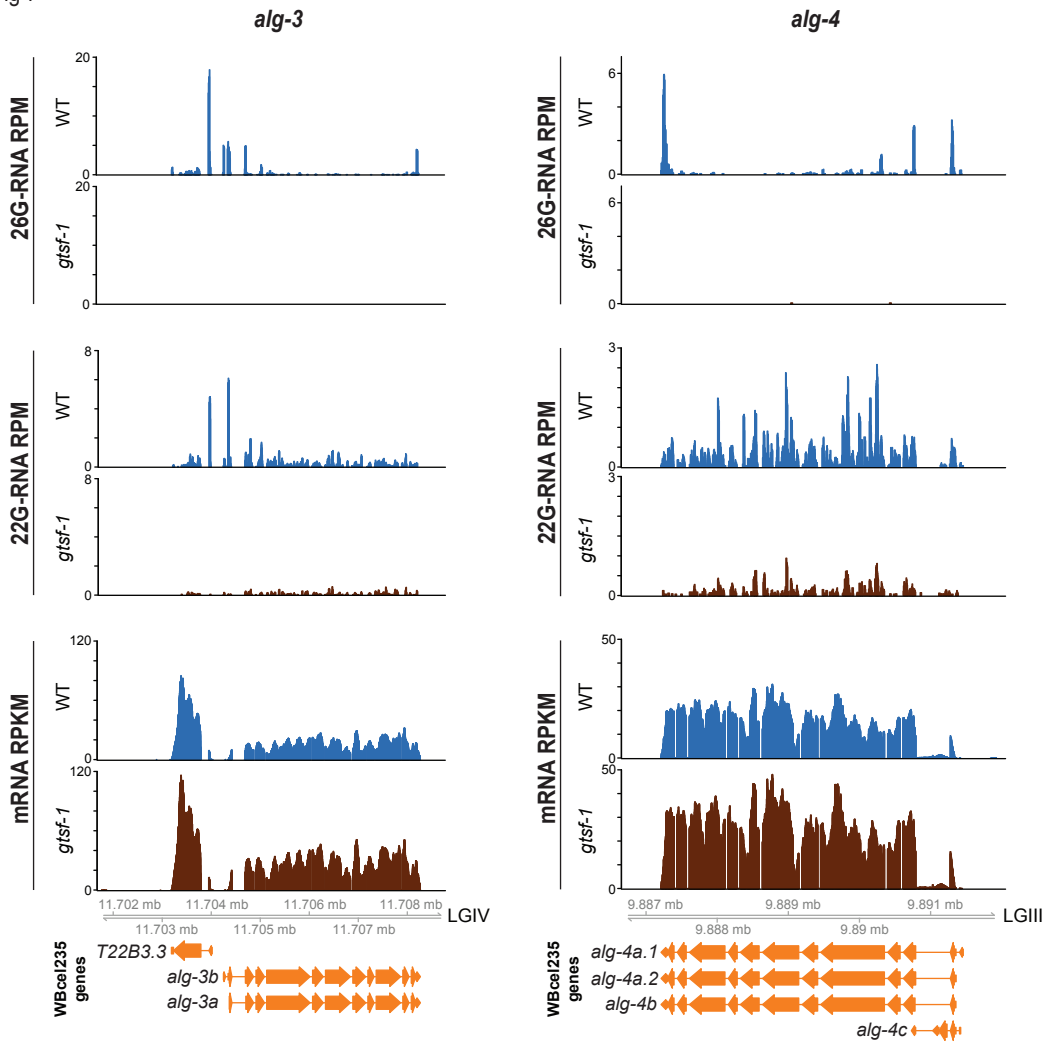
alg-3
alg-4
26G-RNA RPM
22G-RNA RPM
mRNA RPKM
WT
gtsf-1
20
0
6
8
3
120
50
11.702 mb
11.703 mb
11.704 mb
11.705 mb
11.706 mb
11.707 mb
11.708 mb
LGIV
9.887 mb
9.888 mb
9.889 mb
9.89 mb
9.891 mb
LGIII
WBcel235 genes
T22B3.3
alg-3b
alg-3a
alg-4a.1
alg-4a.2
alg-4b
alg-4c

S1 Fig

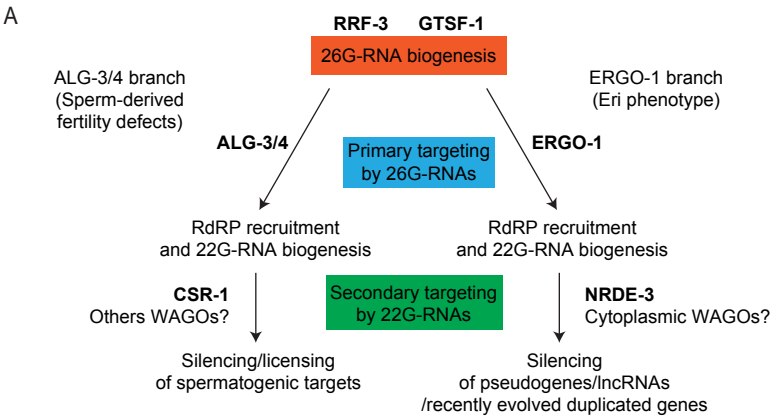

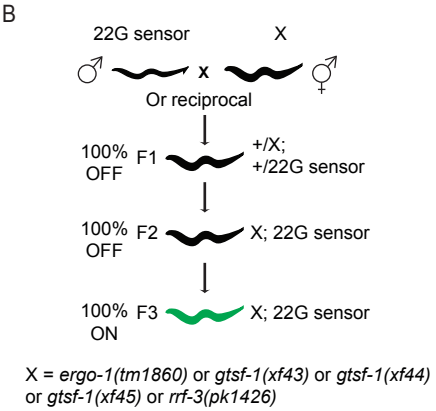

X = *ergo-1(tm1860)* or *gtsf-1(xf43)* or *gtsf-1(xf44)* or *gtsf-1(xf45)* or *rrf-3(pk1426)*

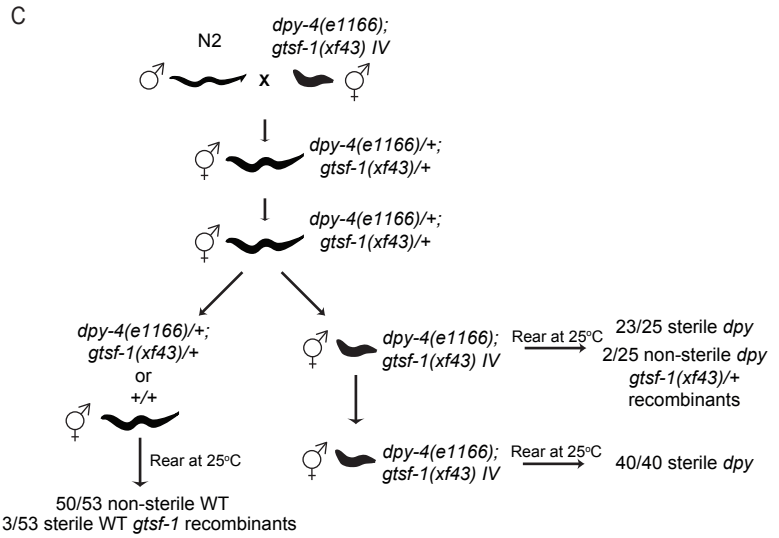

S2 Fig

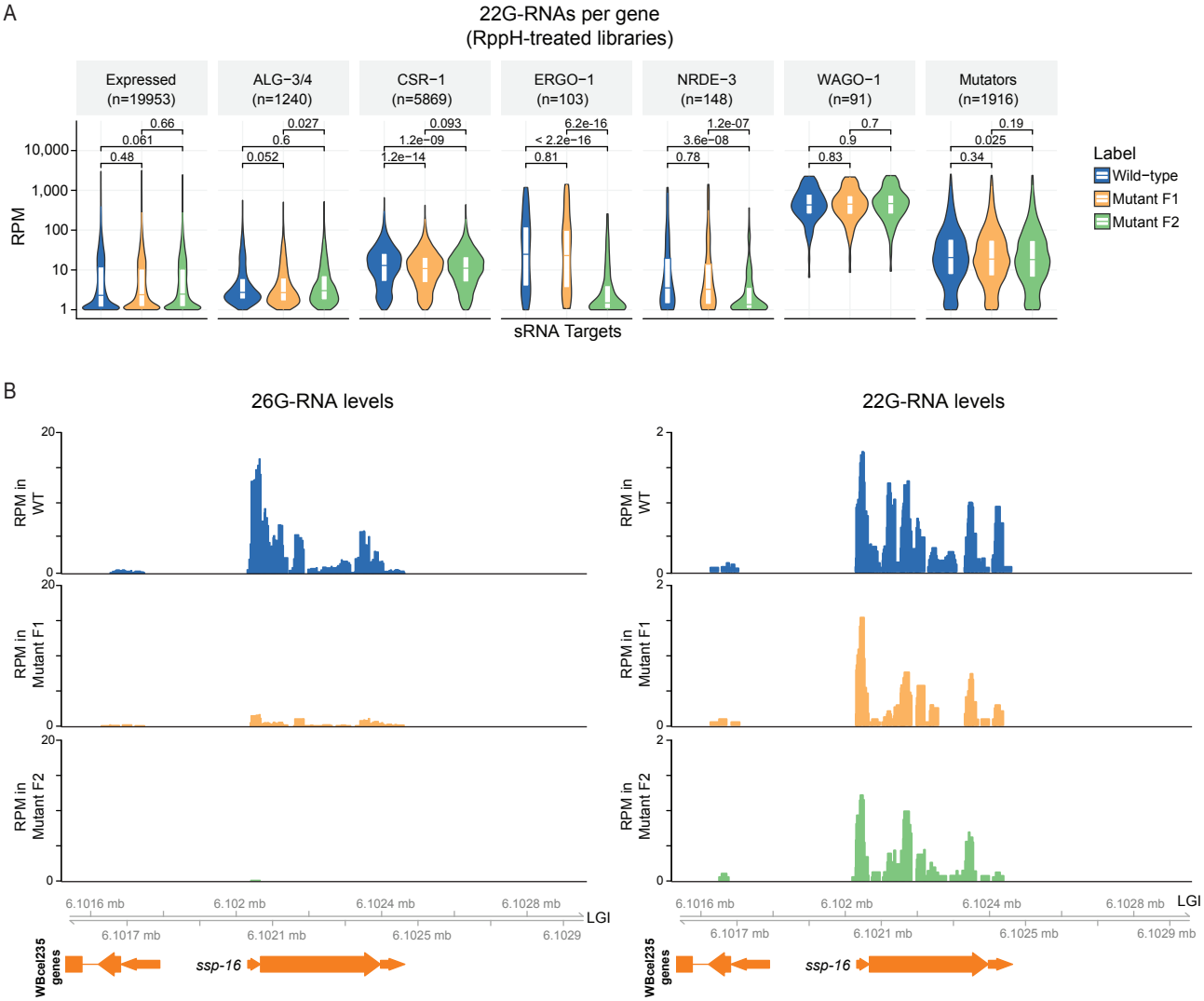

S3 Fig

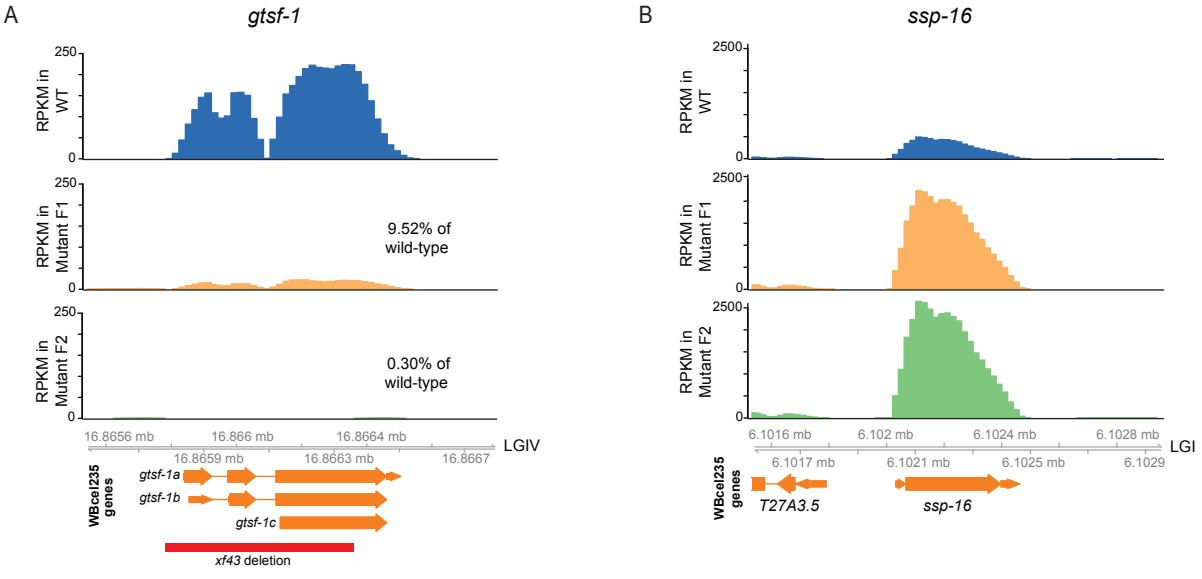
A
gtsf-1
RPKM in WT
250
0
RPKM in Mutant F1
250
0
9.52% of wild-type
RPKM in Mutant F2
250
0
0.30% of wild-type
16.8656 mb
16.866 mb
16.8664 mb
LGIV
16.8659 mb
16.8663 mb
16.8667
WBcel235 genes
gtsf-1a
gtsf-1b
gtsf-1c
xf43 deletion
B
ssp-16
RPKM in WT
2500
0
RPKM in Mutant F1
2500
0
RPKM in Mutant F2
2500
0
6.1016 mb
6.102 mb
6.1024 mb
6.1028 mb
LGI
6.1017 mb
6.1021 mb
6.1025 mb
6.1029
WBcel235 genes
T27A3.5
ssp-16

S4 Fig

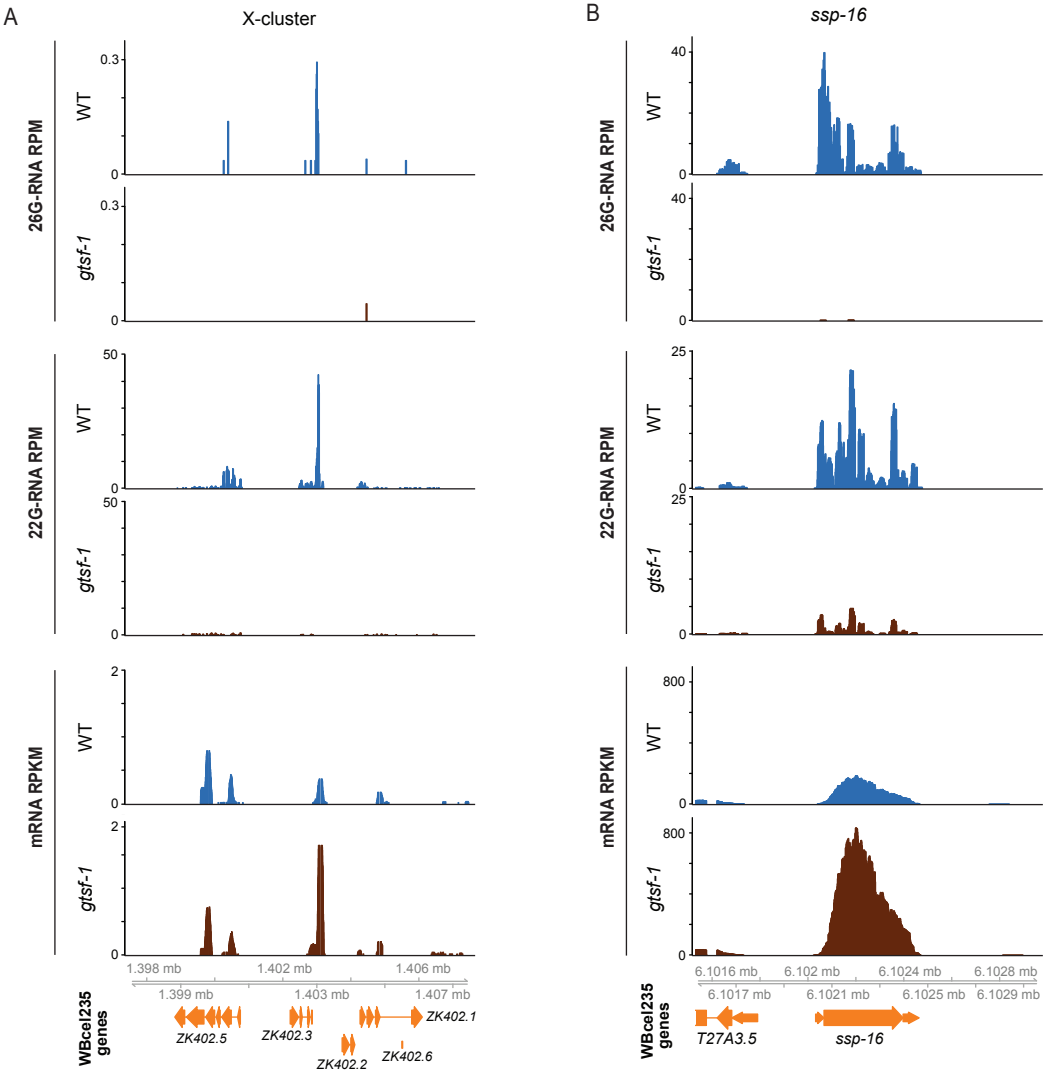
A
X-cluster
B
ssp-16
26G-RNA RPM
22G-RNA RPM
mRNA RPKM
WT
gtsf-1
0.3
0
50
2
40
25
800
1.398 mb
1.402 mb
1.406 mb
1.399 mb
1.403 mb
1.407 mb
ZK402.5
ZK402.3
ZK402.1
ZK402.2
ZK402.6
6.1016 mb
6.102 mb
6.1024 mb
6.1028 mb
6.1017 mb
6.1021 mb
6.1025 mb
6.1029 mb
T27A3.5
ssp-16
WBcel235 genes

S5 Fig

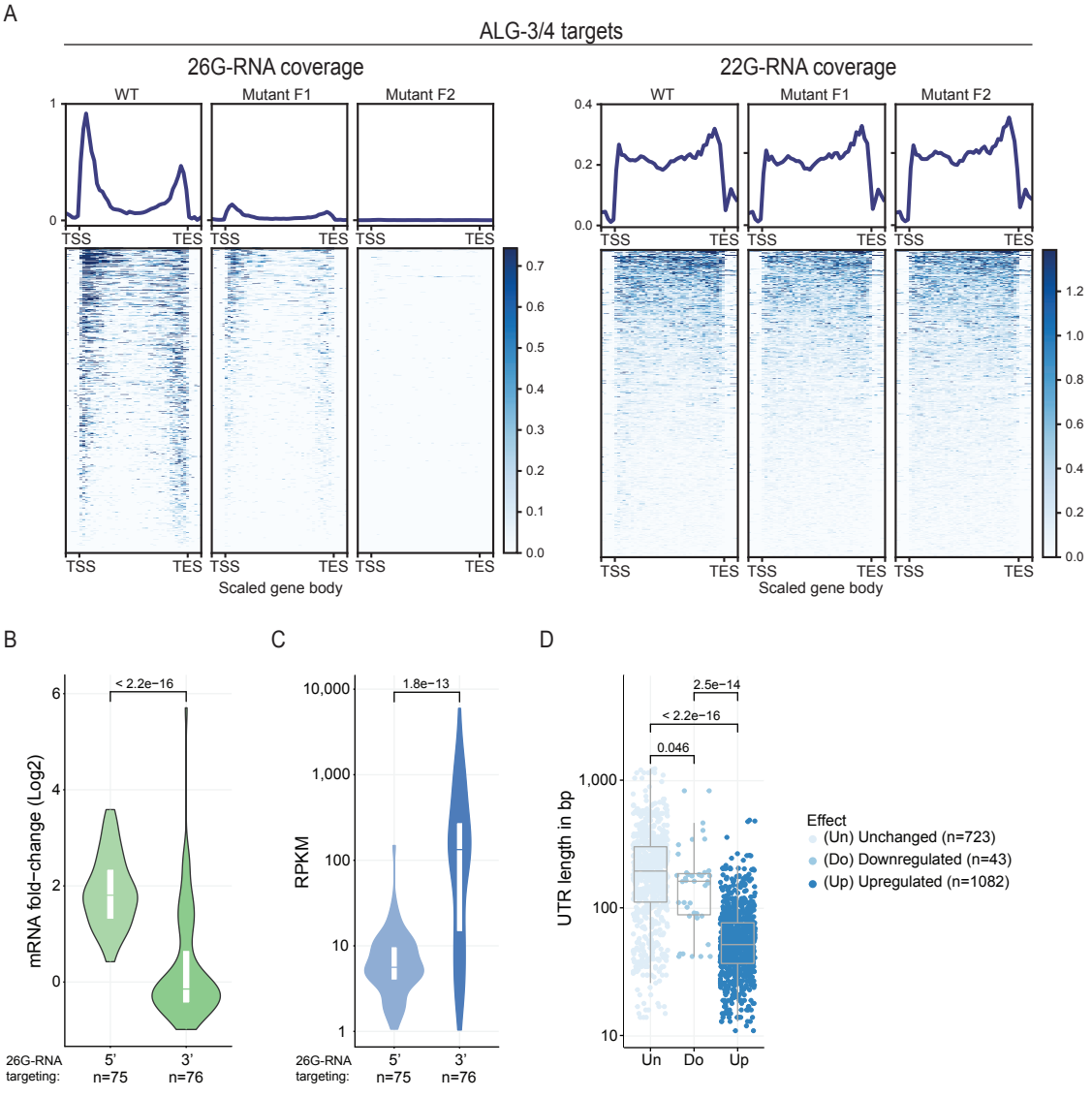
A
ALG-3/4 targets
26G-RNA coverage
22G-RNA coverage
WT
Mutant F1
Mutant F2
TSS
TES
Scaled gene body
B
mRNA fold−change (Log2)
< 2.2e−16
26G-RNA targeting:
5' n=75
3' n=76
C
RPKM
1.8e−13
D
UTR length in bp
2.5e−14
< 2.2e−16
0.046
Un
Do
Up
Effect
(Un) Unchanged (n=723)
(Do) Downregulated (n=43)
(Up) Upregulated (n=1082)

S6 Fig

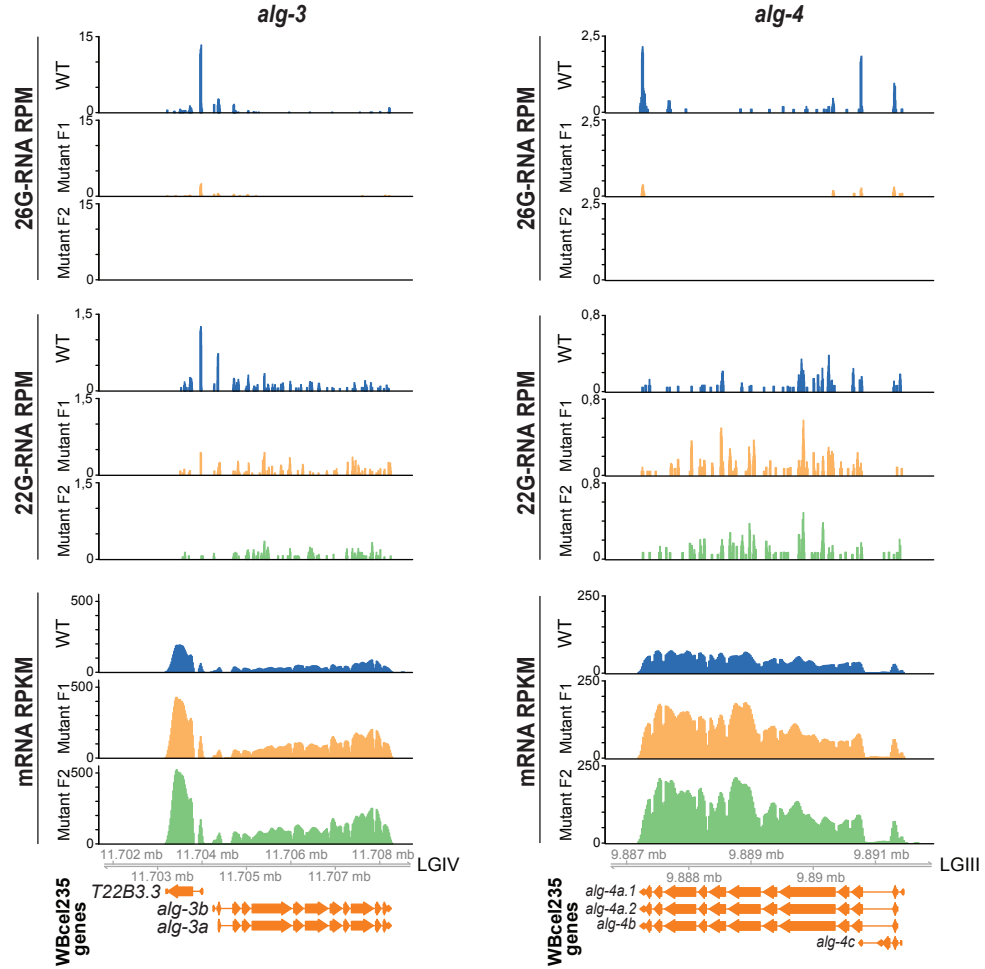
alg-3
alg-4
26G-RNA RPM
22G-RNA RPM
mRNA RPKM
WT
Mutant F1
Mutant F2
15
2,5
1,5
0,8
500
250
0
11.702 mb
11.704 mb
11.706 mb
11.708 mb
11.703 mb
11.705 mb
11.707 mb
LGIV
9.887 mb
9.889 mb
9.891 mb
9.888 mb
9.89 mb
LGIII
WBcel235 genes
T22B3.3
alg-3b
alg-3a
alg-4a.1
alg-4a.2
alg-4b
alg-4c